Renal effects of dapagliflozin in people with and without diabetes with moderate or severe renal dysfunction: prospective modeling of an ongoing clinical trial.

K. Melissa Hallow[1], David W. Boulton[2a], Robert C. Penland[2b], Gabriel Helmlinger[2b], Emily Nieves[1], Daniël H. van Raalte[3], Hiddo L Heerspink[4,5], Peter J. Greasley[6]

1. Department of Chemical, Materials, and Biomedical Engineering, University of Georgia, Athens, GA, USA

2. Clinical Pharmacology and Quantitative Pharmacology, Clinical Pharmacology and Safety Sciences, R&D, AstraZeneca, [a]Gaithersburg, MD, USA, [b]Waltham, MA, USA, [c]Gothenburg, Sweden

3. Diabetes Center, Department of Internal Medicine, Amsterdam University Medical Centers, location VUMC, Amsterdam, The Netherlands

4. Department of Clinical Pharmacy and Pharmacology, University of Groningen, Groningen, Netherlands

5. The George Institute for Global Health, Sydney, Australia

6. Early Clinical Development, Research and Early Development, Cardiovascular, Renal and Metabolism (CVRM) BioPharmaceuticals R&D, AstraZeneca, Gothenburg, Sweden and AstraZeneca R&D, Gothenburg, SE-431 83

Corresponding Author:

K. Melissa Hallow
597 D.W. Brooks Dr.
Athens, GA 30602
Hallowkm@uga.edu

Running Title: Modeling renal effects of dapagliflozin

Pages: 45
Figures: 9
Tables: 3
Abstract Word Count: 249
Introduction Word Count: 556
Discussion Word Count: 1500

JPET Fast Forward. Published on August 6, 2020 as DOI: 10.1124/jpet.120.000040
This article has not been copyedited and formatted. The final version may differ from this version.

ABSTRACT

Sodium Glucose Cotransporter 2 inhibitors (SGLT2i) reduce cardiovascular events and onset and progression of renal disease by mechanisms that remain incompletely understood, but may include clearance of interstitial congestion and reduced glomerular hydrostatic pressure. The ongoing DAPASALT mechanistic clinical study will evaluate natriuretic, diuretic, plasma/extracellular volume and blood pressure responses to dapagliflozin in people with type 2 diabetes (T2D) with normal or impaired renal function (D-PRF and D-IRF, respectively), and in normoglycemic individuals with renal impairment (N-IRF). In this study, a mathematical model of renal physiology, pathophysiology, and pharmacology was used to prospectively predict changes in sodium excretion, blood and interstitial fluid volume (IFV), blood pressure, glomerular filtration rate, and albuminuria in DAPASALT. After validating the model with previous diabetic nephropathy trials, virtual patients were matched to DAPASALT inclusion/exclusion criteria, and the DAPASALT protocol was simulated. Predicted changes in glycosuria, blood pressure, GFR, and albuminuria were consistent with other recent studies in similar populations. Predicted albuminuria reductions were 46% in D-PRF, 34.8% in D-IRF, and 14.2% in N-IRF. The model predicts similarly large IFV reduction between D-PRF and D-IRF, and less but still substantial IFV reduction in N-IRF, even though glycosuria attenuated in groups with impaired renal function. When DAPASALT results become available, comparison with these simulations will provide a basis for evaluating how well we understand the cardiorenal mechanism(s) of SGLT2i. Meanwhile, these simulations link dapagliflozin's renal mechanisms to changes in IFV and renal biomarkers, suggesting these benefits may extend to those with impaired renal function and nondiabetics.

SIGNIFICANCE STATEMENT

Mechanisms of SGLT2 inhibitors' cardiorenal benefits remain incompletely understood. We used a mathematical model of renal physiology/pharmacology to prospectively predict responses to dapagliflozin in the ongoing DAPASALT study. Key predictions include similarly large interstitial fluid

JPET Fast Forward. Published on August 6, 2020 as DOI: 10.1124/jpet.120.000040
This article has not been copyedited and formatted. The final version may differ from this version.

volume (IFV) reductions between subjects with normal and impaired renal function, and less but still substantial IFV reduction in non-diabetics, even though glycosuria is attenuated in these groups. Comparing prospective simulations and study results will assess how well we understand the cardiorenal mechanism(s) of SGLT2i.

Non-standard Abbreviations:

ΔPerm	Change in glomerular membrane permeability
ΔSA	Change in glomerular capillary surface area
η	Fractional Na+ reabsorption
Φ_{glu}	Tubular glucose flow rate
Φ_{Na}	Tubular sodium flow rate
$\mu_{other,seiv}$	Podocyte injury
$\pi_{go\text{-}avg}$	average glomerular capillary oncotic pressure
ACEI	Angiotensin converting enzyme inhibitor
Ang	Angiotensin
ARB	Angiotensin receptor blocker
$C_{albumin}$	Plasma albumin concentration
C_{glu}	Plasma glucose concentration
C_{Na}	Plasma sodium concentration
CD	Collecting duct
DBP	Diastolic blood pressure
D-IRF	Type 2 Diabetics with impaired renal function
D-PRF	Type 2 Diabetics with preserved renal function
eGFR	Estimated glomerular filtration rate
GFR	Glomerular filtration rate
IFV	Interstitial fluid volume
$K_{albumin}$	Glomerular albumin sieving coefficient

K_f	Glomerular ultrafiltration coefficient
MAP	Mean arterial pressure
NHE3	Sodium-hydrogen exchanger 3
N-IRF	Normoglycemic with impaired renal function
P_{Bow}	Bowman's pressure
P_{gc}	Glomerular capillary hydrostatic pressure
PT	Proximal tubule
R_{preaff}	Preafferent arteriole resistance
R_{aff}	Afferent arteriole resistance
RAAS	Renin-angiotensin-aldosterone system
RBF	Renal blood flow
$RC_{albumin}$	Proximal tubule capacity to reabsorb a filtered albumin
RIHP	Renal interstitial hydrostatic pressure
RVR	Renal vascular resistance
$S_{P\text{-}N}$	$_P$ressure-natriuresis sensitivity
SBP	Systolic blood pressure
SEC_{renin}	Renin secretion rate
SGLT2i	Sodium Glucose Cotransporter 2 inhibitor
SNGFR	Single nephron glomerular filtration rate
T2D	Type 2 Diabetes
TGF	Tubuloglomerular feedback
UACR	Urinary albumin creatinine ratio
UAER	Urinary albumin excretion rate
UGE	Urinary glucose excretion
V_b	blood volume

JPET Fast Forward. Published on August 6, 2020 as DOI: 10.1124/jpet.120.000040
This article has not been copyedited and formatted. The final version may differ from this version.

JPET Fast Forward. Published on August 6, 2020 as DOI: 10.1124/jpet.120.000040
This article has not been copyedited and formatted. The final version may differ from this version.

INTRODUCTION

Sodium glucose cotransporter 2 inhibitors (SGLT2i) have been shown to reduce cardiovascular (and particularly heart failure) events and improve renal outcomes in people with type 2 diabetes (T2D) (Zinman et al., 2015; Mosenzon et al., 2019). While SGLT2 inhibition produces an initial hemodynamic drop in GFR, results from EMPA-REG, CANVAS, and DECLARE outcomes trials demonstrated that kidney function in the treated groups stabilized, while the placebo group progressed (Wanner et al., 2016; Guthrie, 2018; Mosenzon et al., 2019). Post-hoc analyses of phase III studies have found that dapagliflozin stabilized estimated GFR (eGFR) decline for up to 2 years (Fioretto et al., 2015) and reduced urinary albumin creatinine ratio (UACR) by 38-48% in those with elevated albuminuria at baseline (Dekkers et al., 2018). Empagliflozin reduced the risk of new onset of macroalbuminuria, doubling of serum creatinine and initiation of dialysis treatment respectively (Wanner et al., 2016).

The mechanisms responsible for these cardiovascular and renoprotective effects remain incompletely understood. Renoprotective mechanisms may include reduced glomerular hydrostatic pressure, reduced proximal tubule sodium transport both directly and through coupled NHE3 inhibition, and/or reduced blood pressure (Hallow et al., 2018). In addition, sodium and glucose excretion with SGLT2i induces an osmotic diuresis which could be responsible for improved heart failure outcomes (Hallow et al., 2017b).

Mathematical modeling provides a tool to describe, test, and quantitatively evaluate proposed mechanisms by which SGLT2 inhibition impacts renal and cardiovascular function. We have previously modeled the renal effects of dapagliflozin and identified a set of mechanisms capable of reproducing urinary and plasma biomarker responses observed in healthy subjects (Hallow et al., 2017b; Hallow et al., 2018). Simulations with this model have demonstrated mathematically that SGLT2i reduces glomerular hydrostatic pressure as an indirect consequence of reduced proximal tubule sodium reabsorption (Vallon and Thomson, 2017). This provides a plausible explanation for the reduction in

albuminuria and slowing of renal progression observed with SGLT2i. In addition, simulations predicted that SGLT2 inhibition will reduce interstitial fluid volume to a greater extent than blood volume, compared to other forms of natriuretic/diuretic agents (Hallow et al., 2018; Mahato et al., 2019). This suggests that in states of volume overload, such as heart failure, SGLT2 inhibition may relieve interstitial congestion without excessive lowering of blood volume and blood pressure, thus maintaining organ perfusion and possibly also preventing excessive neurohormonal activation.

While SGLT2 inhibition has been shown to reduce total body fluid volume, no study has yet distinguished the relative effects of SGLT2 inhibition on blood and interstitial fluid volume during standardized sodium intake. The DAPASALT study (NCT03152084) is an open label, phase IV, three-arm mechanistic study designed to evaluate the natriuretic, diuretic and blood pressure responses to 2-week dapagliflozin treatment in people with T2D with and without renal impairment, and in normoglycemic individuals with renal impairment. Data obtained from this study may allow clinical evaluation of model-based mechanistic hypotheses, including the relatively larger effect on interstitial fluid volume compared to blood volume. The true test of any mathematical model is its ability to prospectively predict behavior. In this analysis, we extend our existing model to prospectively simulate changes in urinary clinical chemistry variables, blood volume, interstitial fluid volume, GFR, and urinary albumin excretion rate (UAER) in the ongoing mechanistic clinical DAPASALT study. This will evaluate the extent to which we truly understand the renal mechanisms of SGLT2i and may also identify gaps in our existing knowledge.

METHODS

Modeling Approach Overview

Using a previously developed mathematical model of renal function and diabetic kidney disease (Hallow et al., 2014; Hallow et al., 2017a; Hallow et al., 2018; Mahato et al., 2019), we generated a population of virtual patients with diabetes and varying degrees of kidney injury by varying model parameters

JPET Fast Forward. Published on August 6, 2020 as DOI: 10.1124/jpet.120.000040
This article has not been copyedited and formatted. The final version may differ from this version.

associated with T2D, hypertension (a common comorbidity with diabetes), and kidney injury. Because the effects of T2D on kidney injury in the model were previously developed based on data from db/db mice with or without uninephrectomy (Mahato et al., 2019), we used human diabetic nephropathy clinical trial data to recalibrate rate constants for this component of the model, and to validate the simulated response to standard-of-care therapies (i.e. ACE inhibitors [ACEI] and angiotensin receptor blockers [ARBs]). We then selected a population of virtual patients to match the DAPASALT inclusion/exclusion criteria and simulated the protocol of the DAPASALT study (NCT03152084).

Model Description

The model of renal function and diabetic kidney injury is summarized in Figure 1 and has been described in detail previously (Hallow and Gebremichael, 2017b; Hallow and Gebremichael, 2017a; Hallow et al., 2018; Mahato et al., 2019). This model describes the key physiological processes of renal function and their roles in maintaining Na^+ and water homeostasis, as well as pathologic processes leading to renal injury and proteinuria in diabetes. Full model equations are also provided in the supplement. Here we provide an overview of the model and describe only key model equations necessary to understand how renal injury and albuminuria were modeled, parameters varied to generate virtual patients, and how SGLT2 inhibition was modeled.

Renal Vasculature*:* As shown in Figure 1A, the kidney is modeled as a set of nephrons in parallel.

Renal blood flow (RBF) is a function of the mean arterial pressure (MAP), renal venous pressure, and renal vascular resistance (RVR), according to Ohm's law (Eq. A1-4 in the supplement). RVR is the equivalent resistance of preafferent, afferent, efferent, and peritubular arterioles and capillaries; it also depends on the number of nephrons.

JPET Fast Forward. Published on August 6, 2020 as DOI: 10.1124/jpet.120.000040
This article has not been copyedited and formatted. The final version may differ from this version.

Glomerular Filtration: Single nephron glomerular filtration rate (SNGFR) depends on the glomerular ultrafiltration coefficient (K_f) as well as the net filtration pressure across the glomerulus, according to Starling's equation:

$$SNGFR = K_f \left(P_{gc} - P_{Bow} - \pi_{go-avg} \right) \quad \text{Eq. 1}$$

Here K_f is the glomerular ultrafiltration coefficient, P_{gc} is glomerular capillary hydrostatic pressure, P_{Bow} is pressure in the Bowman's space, and $\pi_{go\text{-}avg}$ is average glomerular capillary oncotic pressure. The total GFR is then the SNGFR multiplied by the number of nephrons:

$$GFR = SNGFR * N_{nephrons} \quad \text{Eq. 2}$$

Glucose filtration, reabsorption, and excretion: Glucose is filtered freely through the glomerulus. Thus, the filtered load for a single nephron is the product of SNGFR and average plasma glucose concentration (C_{glu}):

$$\Phi_{glu,filtered} = SNGFR * C_{glu} \quad \text{Eq. 3}$$

Glucose is reabsorbed by SGLT2 in the S1 and S2 segments of the proximal tubule (PT) and by SGLT1 in the S3 segment, up to the reabsorptive capacity of each segment (Eq. A8-9). Any unreabsorbed glucose then flows through the rest of the tubule and is excreted in the urine (Eq. A10).

Na^+ filtration and reabsorption: The single nephron filtered Na^+ load is given by:

$$\Phi_{\mathrm{Na,filtered}} = SNGFR * C_{Na} \quad \text{Eq. 4}$$

where C_{Na} is the plasma Na^+ concentration. Na+ is reabsorbed through different transporters at different rates in each segment along the tubule. In the proximal tubule, NHE3 plays a major role in Na+ reabsorption, and thus NHE3 reabsorption is modeled explicitly. In addition, coupling of Na+ reabsorption is Glucose and Na^+ are reabsorption through SGLT2 at a 1:1 molar ratio (Eqs. A12) and by SGLT1 at a 1:2 molar ratio (Eq. A13) is modeled. Additional Na+ reabsorption through other transporters

is also accounted for (Eq. A14). For the remaining nephron segments, we approximate Na^+ reabsorption in each segment as distributed uniformly along the length and defined by a fractional rate of reabsorption, Eq. A15-18.

Dapagliflozin treatment is not associated with changes in serum potassium, and so for simplicity, potassium filtration and reabsorption was not tracked in the model (Yavin et al., 2016).

Water reabsorption: Water reabsorption in the PT is isosmotic. Thus, the rate of water reabsorption depends on the concentration of osmolytes, including Na+ and glucose, in the tubular fluid (Eq. A19-21).

The flow rate of osmolytes and water out of the PT are then used to determine water reabsorption along the remaining nephron segments, including regulation by vasopressin in the collecting duct, as described previously and in the supplement (Eq. A22-28).

Blood and Interstitial Fluid and peripheral sodium storage: Sodium and water are modeled as distributed between the blood, interstitium, and a third compartment that stores Na^+ non-osmotically (Figure 1B) (Titze, 2009; Titze, 2014; Hammon et al., 2015; Hallow et al., 2017b). Sodium and water are assumed to move freely between the blood and interstitial fluid across a Na^+ concentration gradient. Water and sodium intake rates are assumed constant. Then blood volume (V_b) and blood sodium (Na_{blood}) are the balance between intake and excretion of water and sodium respectively, and the intercompartmental transfer between blood and interstitium (Eq. A29-30). Similarly, interstitial fluid volume (IFV) depends on the intercompartmental transfer between blood and interstitium (Eq. A31).

When interstitial sodium concentration exceeds the normal equilibrium level, Na+ is assumed to move out of the interstitium and is sequestered in the peripheral Na+ compartment, where it is osmotically inactive. Thus, the change in interstitial fluid sodium depends on intercompartmental transfer and peripheral storage (Eq. A32-34). Sodium cannot be stored indefinitely, and thus there is a limit on how much sodium can be stored.

JPET Fast Forward. Published on August 6, 2020 as DOI: 10.1124/jpet.120.000040
This article has not been copyedited and formatted. The final version may differ from this version.

Albumin filtration, reabsorption, and excretion: The rate of albumin filtration is a function of SNGFR, the plasma albumin concentration $C_{albumin}$, and the sieving coefficient $K_{albumin}$, as described in (Lazzara and Deen, 2007):

$$\Phi_{albumin,filtered} = K_{albumin} * SNGFR * C_{albumin} \quad \text{Eq. 5}$$

The PT has limited capacity to reabsorb a filtered albumin ($RC_{albumin}$), beyond which excess albumin is excreted.

$$\Phi_{albumin,reabs} = min\left(\Phi_{albumin,filtered}, RC_{albumin}\right) \quad \text{Eq. 6}$$

The urinary albumin excretion rate (UAER) is then:

$$UAER = \left(\Phi_{albumin,filtered} - \Phi_{albumin,reabs}\right) * N_{nephrons} \quad \text{Eq. 7}$$

Kidney injury: Nephron loss due to kidney injury was modeled by reducing the number of nephrons $N_{nephrons}$. While nephron loss in kidney disease is progressive, we did not account for progressive nephron loss in the current analysis, since all simulation durations were less than 6 months.

We assumed that, when glomerular capillary hydrostatic pressure P_{gc} rises above some normal limit $P_{gc,0}$, it causes injury and dysfunction of the glomerulus and podocytes. The magnitude of this injury signal is defined as:

$$GP_{injury} = \max(P_{gc} - P_{gc0}, 0) \quad \text{Eq. 8}$$

Glomerular hypertension causes glomerular hypertrophy, with up to a 50% increase in glomerular volume observed within a few weeks in diabetic and/or nephrectomized rats, mice, and humans (Flyvbjerg et al., 2002; Levine et al., 2008; Bivona et al., 2011). The ultra-filtration coefficient K_f, in Eq. 1 above, reflects both the permeability and surface area of the glomerular membrane. The effect of

JPET Fast Forward. Published on August 6, 2020 as DOI: 10.1124/jpet.120.000040
This article has not been copyedited and formatted. The final version may differ from this version.

glomerular hypertension on K_f through changes in the glomerular surface area (hypertrophy) is modeled as:

$$\frac{d}{dt}(\Delta SA) = (\Delta SA_{max} - \Delta SA) * \frac{GP_{injury}}{\tau_{SA}} \quad \text{Eq. 9}$$

ΔSA_{max} is the maximum increase in glomerular surface area (SA; expressed as a percentage). and τ_{SA} represents the time constant for the increase in surface area. ΔSA_{max} is fixed at 50%, and the time constant τ_{SA} is set so that a steady-state is reached within a few weeks.

Glomerular hypertension also contributes to progressive glomerulosclerosis, a slower process than glomerular hypertrophy. Mathematically, this can be represented as a decrease in glomerular permeability ΔPerm, so that the ultrafiltration coefficient K_f is given by:

$$K_f = K_{f,0} * (1 + \Delta SA - \Delta Perm) \quad \text{Eq. 10}$$

where $K_{f,0}$ is the normal ultrafiltration coefficient in the healthy state. For this analysis, we assume that progression of glomerulosclerosis over the simulation period (6 months of less) is minimal. Thus, ΔPerm is treated as a parameter representing damage that has already accrued, but does not change during the simulation.

Glomerular hypertension also damages to podocytes, causing them to leak protein. Reversible glomerular hypertensive injury to podocytes is modeled as a sigmoidal function:

$$\mu_{gp,seiv} = \frac{E_{max} GP_{injury}^{\gamma}}{GP_{injury}^{\gamma} - K_{m,gp,seiv}^{\gamma}} \quad \text{Eq. 11}$$

There may some podocyte injury that is irreversible, or that is due to non-hemodynamic mechanisms. This is represented by a parameter $\mu_{other,siev}$. The albumin sieving coefficient is then given by

$$K_{albumin} = K_{albumino} * (1 + \mu_{gp,seiv} + \mu_{other,seiv}) \quad \text{Eq. 12}$$

JPET Fast Forward. Published on August 6, 2020 as DOI: 10.1124/jpet.120.000040
This article has not been copyedited and formatted. The final version may differ from this version.

$K_{albumin,0}$ is the sieving coefficient under normal conditions. Changes in albumin excretion are assumed to reflect near instantaneous, within hours to days, changes in glomerular hypertension. This is consistent with the fast changes in proteinuria observed with antihypertensive treatments, and in diseases such as preeclampsia (Mikami et al., 2014).

Regulatory mechanisms: The model incorporates key intrinsic and neurohormonal regulatory feedback mechanisms, as illustrated in Figure 1D. 1) Tubuloglomerular feedback (TGF) is modeled as a signal from macula densa sodium flow (Eq. A45) that signals the afferent arteriole (Eq. A1) to constrict or relax. 2) Myogenic autoregulation is modeled as a function of preafferent pressure (Eq. A46-47) that signals the preafferent arterioles (Eq. A1) to constrict or relax. 3) Vasopressin is modeled as a function of plasma Na^+ concentration (Eq. A48) that alters collecting duct water reabsorption (Eq. A25). 4) The pressure-natriuresis phenomenon is modeled as a signal from renal interstitial hydrostatic pressure (Eq. 49-50) that alters Na^+ reabsorption rates along the nephron (Eq. A14, A16). 5) Whole-body blood flow autoregulation is modeled as a signal from cardiac output that modulates peripheral resistance (Eq. A51, Eq. 12). 6) To describe the Renin-Angiotensin-Aldosterone System (RAAS), renin secretion is modeled as a function of macula densa sodium flow, with a strong inhibitory feedback from Angiotensin II (AngII) bound to the AT1 receptor (AT1-bound AngII) (Eq. A52-55). Renin generates Angiotensin I, which can be converted to AngII by ACE or chymase or degraded (Eq. A56). AngII can bind to the AT1 or AT2 receptor or can be degraded (Eq. A57). AT1-bound AngII signals efferent, preafferent, and afferent vasoconstriction, PT sodium retention, and aldosterone secretion (Eq. A59). Aldosterone binds to the mineralocorticoid receptor (Eq. A60) and signals sodium retention in the connecting tubule/collecting duct (Eq. A61).

SGLT2 inhibition: As described previously, the direct effect of 10 mg once daily dapagliflozin on SGLT2 was modeled as a constant 85.3% inhibitory effect on the glucose reabsorption rate per unit length through SGLT2 in the S1 and S2 segments (Eq. S68, utilized above in Eq. S8)(Hallow et al., 2018). After

JPET Fast Forward. Published on August 6, 2020 as DOI: 10.1124/jpet.120.000040
This article has not been copyedited and formatted. The final version may differ from this version.

initiating treatment with SGLT2i, urinary glucose excretion (UGE) reaches a maximum within 24 hours, and then settles to a stable level slightly less than peak over next several days. This is assumed to be in part due to compensation as SGLT1 and 2 are upregulated, and as described previously (Hallow et al., 2018), we assumed unreabsorbed glucose signals upregulation of SGLT, up to a maximum increase in activity of 30% (Eq. S68-70). Lastly, SGLT2i is assumed to have a weak inhibitory effect on Na+ reabsorption through NHE3 (Fu et al., 2014; Pessoa et al., 2014; Coady et al., 2017) (Eq. S71). We previously showed that 8% inhibition of NHE3 with SGLT2i is sufficient to explain observed electrolyte excretion responses to SGLT2i(Hallow et al., 2018).

Technical implementation

The model was implemented in the open-source programming software R 3.1.2, using the *RxODE* package (Wang et al., 2016). Prior to availability of trial results, simulation results were placed in an online repository at https://bitbucket.org/hallowkm/dapasalt/src/master/, which provides time-stamping of the results.

Virtual Patient Generation

Baseline model parameters are given in Tables S1-5. A population of 4000 virtual patients was generated by random sampling of a subset of model parameters over the ranges listed in Table 1. Because the distributions of these parameters within the population are generally unknown, a uniform distribution was used. Parameters to be sampled were chosen based on their mechanistic role of diabetes, kidney injury, and hypertension. Diabetes was simulated by increasing average plasma glucose concentration C_{glu} over a range of 7.8 to 14 mmol/L (corresponding to HbA1c of 6.5% to 10.5%). Existing glomerulosclerosis and nephron loss were represented by varying the initial conditions for pressure-induced reductions in glomerular permeability (ΔPerm) and for nephron loss (Δnephrons), respectively. Here, 0% represents no injury and 100% represents complete loss of glomerular permeability or

nephrons, respectively. Podocyte injury ($\mu_{other,seiv}$) and PT albumin reabsorptive capacity ($RC_{albumin}$), were also varied. Ranges for these parameters were chosen such that the resulting proteinuria ranged from zero to 10 grams/day. Hypertension was simulated by varying preafferent and afferent arteriole resistances (R_{preaff} and R_{aff}), PT and collecting duct fractional Na+ reabsorption (η_{pt} and η_{cd}), and pressure-natriuresis sensitivity ($S_{P\text{-}N}$) and setpoint ($RIHP_0$), as previously described (Hallow et al., 2014; Hallow and Gebremichael, 2017a). Sodium intake ($\Phi_{Na,in}$) was also sampled to represent normal population variability in sodium intake. Baseline renin and aldosterone secretion ($SEC_{renin,0}$, $Aldo_0$) were varied to produce variability in baseline renin and aldosterone concentrations. After simulating to a new steady-state, virtual patient values for key clinical measures were compared with physiologically reasonable values, and virtual patients with values falling outside of those ranges were rejected.

Model Calibration and Validation with Diabetic Nephropathy Clinical Trials

We have previously described calibration and validation of several key model behaviors: 1) We have calibrated the model to describe observed blood pressure reduction and plasma renin changes in response to antihypertensive therapies (ACE inhibitors [ACEi] including enalapril, Angiotensin Receptor Blockers [ARBs] including losartan, renin inhibitors, thiazide diuretics, and calcium channel blockers), and have shown that it is able to predict the response to combinations of these drugs (Hallow et al., 2014; Hallow and Gebremichael, 2017a). 2) We have shown that the model is able to describe clinically observed changes in urinary glucose, sodium, and volume, changes in plasma sodium and creatinine, and changes in blood pressure in response to SGLT2 inhibition (Hallow et al., 2018). 3) In addition, we previously demonstrated that the model describes progression of albuminuria, hyperfiltration, and GFR decline in murine diabetes models (Mahato et al., 2019). However, the ability of the model to describe the effects of pharmacologic intervention in diabetic nephropathy patients has not previously been demonstrated. To this end, we simulated several key clinical trials in diabetic nephropathy (RENAAL

(Brenner et al., 2001), IDNT (Lewis et al., 2001), NESTOR (Marre et al., 2004), and AVOID (Parving et al., 2008)), focusing on the short-term (<= 6 months) albuminuria and GFR changes. Over this time period, GFR changes are likely due primarily to renal hemodynamic alterations rather than changes in disease progression (Holtkamp et al., 2011). In this analysis, we did not attempt to predict renal outcomes or long-term changes in GFR.

Each study represents a different segment of the diabetic nephropathy population and/or a different treatment regimen. RENAAL and IDNT investigated ARBs losartan and irbesartan, respectively, in patients with macroalbuminuria and low eGFR. IDNT also required that patients were hypertensive at baseline. NESTOR evaluated the ACEi enalapril in patients with microalbuminuria and moderate eGFR. In these three studies, any prior ACEi or ARB treatment was discontinued before randomization. The AVOID study investigated the addition of the renin inhibitor aliskiren to background ARB (losartan) in patients with macroalbuminuria. However, baseline albuminuria was less severe than in RENAAL and IDNT, and baseline eGFR fell between that of RENAAL/IDNT and NESTOR.

RENAAL was used as a calibration study, and model parameters previously calibrated using mouse data (specifically, parameters in Eq. 11 defining the relationship between glomerular hydrostatic pressure and protein sieving injury) were refined to improve the fit to the RENAAL UACR data. No other model parameters required adjustment. Then IDNT, NESTOR, and AVOID were simulated, and results were compared with reported changes in albuminuria and eGFR. It should be noted that while the model calculates GFR directly (Equations 1-2), these studies estimated GFR based on serum creatinine. Formulas for estimating GFR are most accurate for GFR less than 60 ml/min.

Clinical Trial Simulation:

For each simulated study, a subset of virtual patients was selected from the full population of virtual patients based on the trial's inclusion and exclusion criteria for HbA1c/blood glucose, UAER or urinary

albumin creatine ratio (UACR), GFR, and MAP. If more than 70% of patients in the trial were on a background antihypertensive therapy, a run-in period with that therapy was simulated before selecting the trial virtual patients. Controlled sodium intake during a run-in period was modeled when specified in the trial protocol. Treatment with study drug and dose was simulated for the trial duration or for 12 months, whichever was shortest.

Summary of Calibration/Validation Studies:

RENAAL was a randomized double-blind placebo-controlled study of losartan in patient with type 2 diabetes (T2D) and nephropathy (UACR > 300mg/g, serum creatinine 1.3 to 3 mg/dl) (Brenner et al., 2001; de Zeeuw et al., 2004). If patients were taking ACEi or ARBs at screening, these medications were discontinued and replaced by alternative antihypertensive medications (primarily diuretics and calcium channel blockers). 1513 patients were randomized to 50 mg losartan or placebo once daily, and uptitrated to 100mg after four weeks if blood pressure remained above target levels. The mean follow-up time was 3.4 years. Only changes in UACR and eGFR at 12 months were used in the current analysis.

IDNT was a randomized double-blind placebo-controlled study of irbesartan in patient with T2D, hypertension (SBP > 135 mmHg, DBP > 85mmHg, or documented treatment with antihypertensive), proteinuria (protein excretion > 900 mg/24 hr), and serum creatinine 1 to 3 mg/dl in women and 1.2 – 3mg/dl in men (Lewis et al., 2001). All ACEi, ARBs, and CCBs were discontinued for at least 10 days before screening and replaced with other agents. 1715 patients were randomized to irbesartan titrated from 2.5 to 10 mg per day or to placebo. The mean follow-up time was 2.6 years. Only changes in UACR and eGFR at 12 months were used in the current analysis.

NESTOR was a 1-year randomized double-blind placebo-controlled study of enalapril or the diuretic indapamine slow release in patients with T2D, microalbuminuria (UAER 28.8 – 288 mg/day), and hypertension (SBP 140-180 mmHg and DBP < 110 mmHg) (Marre et al., 2004). All ACEi, ARBs, and CCBs

JPET Fast Forward. Published on August 6, 2020 as DOI: 10.1124/jpet.120.000040
This article has not been copyedited and formatted. The final version may differ from this version.

were discontinued before randomization. 570 patients were randomized to one of three groups: enalapril 10mg, indapamine 1.5 mg sustained release, or placebo.

AVOID was a 6-month randomized double-blind placebo-controlled study of aliskiren added to 100mg losartan in patients with T2D and macroalbuminuria (UACR > 300 mg/g) (Lewis et al., 2001). Inclusion criteria included eGFR > 30 ml/min/1.73m^2 and serum creatinine 1 to 3 mg/dl in women and 1.2 – 3mg/dl in men. During a 3-month run-in period, all RAAS blockers were discontinued and replaced with 100mg losartan daily, plus additional antihypertensives as needed to achieve target blood pressure of < 130/80 mmHg. 599 patients were randomized to aliskiren 150mg uptitrated to 300mg at 12 weeks, or to placebo.

DAPASALT Study Protocol: DAPASALT is an open label, mechanistic, three-arm study to evaluate the natriuretic effect of 2-week dapagliflozin treatment with participants on a fixed sodium diet. The study population consists of three groups of patients (Caucasians, age 18-75 years of age) with either 1) T2D without renal impairment (HbA1c 6.5-10%, eGFR 90-130 ml/min/1.73m^2), 2) T2D with impaired renal function (HbA1c 6.5-10%, eGFR 25-50 ml/min/1.73m^2), or 3) normoglycemic individuals with impaired renal function (eGFR 25-50 ml/min/1.73m^2) and confirmed diagnosis of focal segmental glomerular sclerosis (FSGS), IgA nephropathy (IgAN), or membranous glomerular nephropathy (MGN). For inclusion, patients must also have been treated with an angiotensin receptor blocker (ARB) for at least 6 weeks prior to starting the trial, and for the individuals with T2D, a stable dose(s) of appropriate glucose-lowering medications other than SGLT2i must be present. Patients must also have stable urinary sodium excretion on two successive 24 hr measures during the run-in period. Patients with systolic and diastolic blood pressure above 160/110 mmHg, respectively, were excluded. Full inclusion and exclusion criteria are included in the supplemental material. The study aims to enroll 51 patients, 17 per arm, to ensure that 15 patients complete each arm. A 2-week screening and run-in period precedes the active treatment period, and patients receive standardized meals with a sodium content of 150 mmol/day,

starting at day -6 and continuing through the study. Subjects receive dapagliflozin 10mg daily for 14 days, followed by a 4-day washout period. The washout period was not considered in the analysis presented here. Study endpoints are given in Table 2. Plasma volume will be measured by indocyanine green distribution and extracellular fluid volume will be measured by bioimpedance spectroscopy analysis.

Results:

Virtual patient population

Of the 4000 potential virtual patients generated, 3389 had physiologically reasonable steady-state values (MAP 70 – 160 mmHg, GFR 15-150 ml/min, UAER 0-10000 mg/day) and were considered acceptable. As shown in Figure 2, top row, the distributions of baseline GFR, MAP, and UACR in the acceptable virtual patient population covered a wide range, providing a cohortfrom which to sample clinical trial populations. UAER was lognormally distributed and GFR and MAP were normally distributed. Table 3 summarizes the number of microalbuminuric, macroalbuminuric, and hypertensive virtual patients within each GFR category. As expected, GFR was lower and SNGFR was higher in virtual patients with greater nephron loss (Figure 3A). Virtual patients with higher glomerulosclerosis tended to have lower GFR, although some virtual patients had low GFR with minimal glomerulosclerosis (Figure 3B). Blood glucose was not associated with GFR (Figure 3C). UAER increased with moderate nephron loss but decreased again as nephron loss increased further (Figure 3D). UAER tended to be higher in virtual patients with more glomerulosclerosis (Figure 3E), and there was no association between blood glucose and UAER (Figure 3F).

To replicate trials in which patients were on an ARB therapy at baseline (AVOID and DAPASALT), virtual patients were simulated on an ARB to reach a new baseline. As shown in Figure 2, bottom row, this

shifted the virtual population distributions of UAER, GFR, and MAP to the left, but the full range of each variable was still covered.

Calibration and Validation: Simulation of previous diabetic nephropathy clinical trials

After selecting study populations from the larger virtual population by applying each trial's inclusion/exclusion criteria for albuminuria and eGFR, the virtual study populations produced were reasonably representative of the clinically reported baseline albuminuria and eGFR measures in each study (Figure 4 A and B). There was heterogeneity across studies in albuminuria measurement used (UACR or UAER) and statistic reported (geometric mean or median, standard deviation, interquartile range, or 95% confidence interval), and we did not explicitly try to fit these values.

The simulated response for each trial also reproduced the reported reductions in albuminuria and eGFR. For RENAAL, model parameters were optimized to fit the observed albuminuria response. For the remaining studies, the model-predicted response reasonably reproduced the observed changes in albuminuria and eGFR. One exception to this was the AVOID GFR response. This study showed a placebo-adjusted increase in eGFR - a finding that is inconsistent with a considerable body of studies showing reductions in eGFR with RAAS blockade, both alone and in combination (Mann et al., 2008; Holtkamp et al., 2011). However, it should be noted that the model does not reproduce this unexpected behavior.

Prospective simulation of DAPASALT

Figure 5 shows the virtual study populations for each arm in DAPASALT. The arms for T2D with preserved renal function, T2D with impaired renal function, and normoglycemic with impaired renal function will be referred to here as D-PRF, D-IRF, and N-IRF. There were no inclusion/exclusion criteria

JPET Fast Forward. Published on August 6, 2020 as DOI: 10.1124/jpet.120.000040
This article has not been copyedited and formatted. The final version may differ from this version.

for UAER. Although each arm of the DAPASALT study will include 15-17 subjects, a larger number of virtual patients were included in the virtual population, to allow the model to capture the full range of responses that might be observed.

Figures 6-8 show the simulated time course of key endpoints measured in the study for each of the three study arms, and Figure 9 compares the response between the three groups at key timepoints. The washout period was not simulated. As expected, predicted 24 hr UGE is highest in the D-PRF group, lower in D-IRF, and lowest in N-IRF (median 94.6, 35.9, and 19.7 g/day on day 14, respectively). In all groups, 24 hour Na^+ excretion is predicted to peak on day 1, overcompensate and dip just below baseline on day 2, and then quickly return to baseline as the virtual patients again reached Na^+ balance. Water excretion is also predicted to peak on day 1, but subsequently to normalize more slowly than Na^+ excretion. In addition, water excretion is predicted to take longer to return to baseline in renally impaired groups (around day 14) compared to the normal renal function group (around day 7).

Urinary Na+ and water excretion time curves are not tracking in parallel because urinary Na^+ excretion reflects changes in proximal tubule Na^+ reabsorption, while water excretion reflects changes in both the proximal tubule and the distal nephron. Compensatory mechanisms eventually restore both Na^+ and water balance, but mechanisms regulating Na^+ balance (e.g. renin, pressure-natriuresis) achieve balance quicker than mechanisms regulating water balance (mainly vasopressin).

The decrease in MAP in D-PRF is predicted to be slightly larger than in the D-IRF group (-5.1 vs -3.6 mmHg). MAP reduction in the N-IRF group is predicted to be small (1 mmHg).

Our simulations predict that the initial reduction in GFR will be much smaller in the impaired renal function groups (-3.8 and -2.3 ml/min in D-IRF and N-IRF groups, respectively), compared to the D-PRF group (-15.2 ml/min). The initial reduction in GFR also varied widely within the D-PRF group, as indicated

by the width of the interquartile range (Figure 6E). Further analysis showed that the largest drops occurred in hyperfiltering virtual patients (baseline GFR >110 ml/min, analysis not shown).

UAER is predicted to decrease substantially in all three groups. In diabetics, the UAER reduction is predicted to be less but still quite large in the impaired renal function group (34.8%), compared to the normal renal function group (45.8%). A smaller reduction (14.2%) is predicted in the N-IRF group. Our simulations predict that the maximum UAER reduction will occur within 14 days.

As we have modeled previously, reductions in IFV are predicted to be much greater than reductions in blood volume. Predicted blood volume reduction is largest in the D-PRF (210 ml), smaller in D-IRF (150 ml), and smallest in the N-IRF group (40ml). On the other hand, predicted IFV reduction is larger in D-IRF group than in the D-PRF group (1.81 vs 1.68 L), and was still substantially reduced in the N-IRF group (1L). Thus, the ratio of IFV to blood volume reduction is predicted to be larger in the renal impairment groups than in normal renal function.

Discussion

Clinical Implications of Model Predictions

Given the weaker glycosuria response to SGLT2i in patients with renal impairment and in non-diabetics, volume changes resulting from osmotic diuresis with SGLT2i might be expected to be diminished in these populations. However, the model predicts IFV reduction will be similar in T2D with and without renal impairment, and that nondiabetics with renal impairment will see smaller but still substantial IFV reductions, even with much lower UGE. Assuming IFV plays an important role in the cardiovascular benefits of SGLT2i, this is consistent with recent findings of the DAPA-HF study, in which significant

improvements in the primary endpoint (worsening of heart failure or cardiovascular death) were seen across all baseline GFRs and independent of diabetic status (McMurray et al., 2019).

The model also suggests a mechanistic explanation for these predictions. Within a single nephron, predicted changes in water excretion were similar between D-PRF and D-IRF groups. However, because the D-PRF have more functioning nephrons, the initial peak in water excretion in this group was larger (Figure 6). The modeling suggests this causes a larger vasopressin response, which limits further excretion and quickly returns water excretion to baseline. In D-IRF, the predicted initial water excretion and thus vasopressin response is lower, so compensation occurs more slowly, allowing similar total water excretion and thus similar volume changes as in the D-PRF group, even though the initial peak was smaller.

A second finding, which we demonstrated previously in single virtual patients (Hallow et al., 2018), is that glomerular hydrostatic pressure reductions, which likely play a large role in dapagliflozin's renoprotective effects, is predicted to be similar in patients with normal or impaired renal function, while initial GFR drop is expected to be smaller in patients with impaired renal function. The sustained glomerular pressure reduction likely explains why the antiproteinuric effects are sustained in patients with low GFR (Heerspink et al., 2016; Fioretto et al., 2018).

Comparison with Available Data

Although DAPASALT study results are not yet available, several available data support the predicted responses. Our simulations reproduce higher UGE observed in patients with normal vs. impaired renal function (List et al., 2009; Kohan et al., 2014). Predicted 3-5 mmHg MAP reductions are consistent with previous studies (List et al., 2009; Wilding et al., 2009; Ferrannini et al., 2010). The simulations reproduce the well-known initial drop in GFR with SGLT2i initiation. This reversible initial reduction is followed by a much slower rate of GFR decline (Wanner et al., 2016). Our simulations predict the initial

GFR drop with dapagliflozin will be smaller in D-IRF than D-PRF. The predicted magnitude in D-IRF (-3.8 ml/min) is consistent with reported eGFR changes in clinical studies of diabetic chronic kidney disease (CKD). In the DERIVE study, in T2D patients with Stage 3a CKD treated with dapagliflozin, GFR fell by 5 ml/min/1.73m^2 at week 4 (Fioretto et al., 2018). A similar reduction (-4 ml/min/1.73m^2) was observed with canagliflozin at week 6 in T2D with Stage 3 CKD (Yamout et al., 2014). Another small study in patients with more severe CKD (mean eGFR 30.3 ml/min/1.73m^2) found smaller 1.3 ml/min/1.73m^2 reduction. This is consistent with our predicted smaller initial GFR reduction in patients with lower baseline GFR.

Most studies reporting renal function changes with SGLT2i have used serum creatinine to estimate GFR, while a few used inulin clearance or other methods to measure GFR directly. eGFR is accurate for GFR less than 60 ml/min/1.73m^2 but may be less accurate for higher GFRs. Studies reporting eGFR changes in patients without renal impairment have reported reductions of 4-5 ml/min/1.73m^2 (Heerspink et al., 2016), and pooled analyses have shown no dependence of change in eGFR on baseline eGFR (Petrykiv et al., 2017). However, studies that measured GFR directly have found larger reductions. In one study, GFR dropped by 10.8 ml/min initially in patients with T2D and normal renal function treated with dapagliflozin (Lambers Heerspink et al., 2013). Another study reported reductions of 5, 10, 12 ml/min in fasted, euglycemic, and hyperglycemic states, respectively (van Bommel et al., 2019). Cherney and colleagues found that empagliflozin reduced GFR in hyperfiltering Type 1 diabetic patients by 25-45 ml/min/1.73m^2, depending on glycemic state (Cherney et al., 2014). They found no GFR change in non-hyperfiltering patients. The magnitude of changes predicted in the DAPASALT D-PRF group (-15.2 ml/min) are consistent with studies measuring GFR directly, and it is possible that measured changes in eGFR in DAPASALT may underpredict true changes in GFR. Our simulations are also consistent with a larger initial GFR drop in hyperfiltering than non-hyperfiltering patients.

The model-predicted changes in albuminuria are consistent with studies showing consistent proteinuria reduction with SGLT2i. In patients with T2D and moderate renal function (baseline eGFR of 72 – 82 ml/min/1.73m^2, 10 mg dapagliflozin reduced UACR by 45% at week (Heerspink et al., 2016), and reduced 24hr UAER by 36.2% at 6 weeks (Petrykiv et al., 2017). In T2D patients with Stage 3a CKD and albuminuria, UACR fell 30.7% at week 4, and 41.7% by week 12 (Fioretto et al., 2018), while in stage 3b-4 CKD, UACR was reduced 38.4% over 102 weeks. Our predicted reductions of 45% and 35% in T2D with normal and impaired renal function, respectively, are consistent with these findings.

Little data is available on fluid volume changes with SGLT2i. As we predict here and in previous analyses of single virtual patients (Hallow et al., 2017b; Hallow et al., 2018), SGLT2i may elicit much larger relative reductions in IFV than in blood volume. This decongestive effect without excessive reduction in blood pressure and organ perfusion may explain the unexpectedly large benefits on heart failure (Zinman et al., 2015; McMurray et al., 2019). To our knowledge, DAPASALT will be the first to measure changes in both IFV and blood volume in the same study. However, studies have separately reported measures that reflect blood or total extracellular fluid volume change. SGLT2i have consistently been found to increase hematocrit, suggesting blood volume reduction. Hematocrit increases of 1.3% and 2.2% were reported in T2D with normal renal function (Lambers Heerspink et al., 2013; WADA et al., 2019). If red blood cell volume remains constant, the model-predicted changes in blood volume correspond to 1.7% hematocrit increase in T2D with preserved GFR, consistent with these studies. Hematocrit changes may also reflect changes in hematopoiesis (Maruyama et al., 2019), but these effects were not modeled here. Two recent studies used bioimpedance to measure extracellular water changes. Unfortunately, these studies did not report hematocrit, so relative reductions in blood and interstitial volumes cannot be determined. These studies were non-randomized and were not placebo-controlled, and thus should be interpreted with care. Ohara and colleagues reported that extracellular water was reduced by 8.4% in diabetic patients with impaired renal function treated with dapagliflozin

(Ohara et al., 2019), and our simulations predict a 9.5% reduction. A recent observational study in T2D with normal renal function treated with empagliflozin or dapagliflozin reported a smaller reduction (400 ml/1.73 m^2) at day 3. A third study with tofogliflozin showed a 0.3 kg reduction in extracellular water (Kamei et al., 2018). This study surprisingly showed a nonsignificant hematocrit decrease, inconsistent with other studies that showed increased hematocrit.

Model Validation

Models cannot reproduce all aspects of physiology and disease. Making predictions and comparing with clinical data is a way to determine whether the model is "good enough" or whether important mechanisms are missing. We previously showed that the model reproduces biomarker and blood pressure responses to RAAS blockers, diuretics, and calcium channel blockers in hypertension (Hallow et al., 2014), and urinary and serum biomarkers responses to dapagliflozin in normal subjects (Hallow et al., 2018). Here, we further retrospectively validated the kidney injury and albuminuria components of the model by demonstrating reasonable agreement between model predictions and observed changes in albuminuria and eGFR for previous diabetic nephropathy clinical trials. This validation demonstrated that the renal physiology/pathophysiology/pharmacology represented in the model is sufficient for describing responses in this population and provides confidence for making prospective predictions in similar populations treated with SGLT2i.

Limitations

The model captures some but not all sources of variability in SGLT2i response. Thus, predicted interquartile ranges are likely narrower than true interquartile ranges. DAPASALT virtual patients were selected based on inclusion/exclusion criteria. Because we do not know the true baseline characteristics, virtual and real populations may differ. Specifically, because no limits were placed on UACR in the DAPASALT protocol, virtual and real baseline UACR could be quite different, which could impact

predicted treatment responses. Few studies report time courses for albuminuria changes prior to 4 weeks. If the model overestimates the speed of UAER reduction, the 2-week UAER response may be overpredicted. For the normoglycemic arm, we did not distinguish between mechanisms of IgAN, FSGS, or MGN. Once study results are available, comparison of simulated and observed baseline characteristics and responses may provide further information for better modeling these populations.

Conclusions

The model predicts similarly large IFV reduction between D-PRF and D-IRF, and less but still substantial IFV reduction in N-IRF, even though glycosuria attenuated in groups with impaired renal function. When DAPASALT results become available, comparison with these prospective simulations will provide a basis for evaluating how well we understand the renal and volume homeostasis mechanism(s) of SGLT2is generally, and dapagliflozin specifically. If the prospective simulations predict the results well, this will also provide further validation of the model as a tool for future predictions.

Acknowledgements: This study was funded by AstraZeneca Pharmaceuticals

Authorship Contributions:

Participated in research design: Hallow, Boulton, Penland, Helmlinger, Nieves, Heerspink, Greasley

Conducted Experiments: Hallow, Nieves

Contributed new reagents or analytic tools: Hallow

Performed data analysis: Hallow, Nieves

Wrote or contributed to the writing of the manuscript: Hallow, Boulton, Penland, Helmlinger, van Raalte, Heerspink, Greasley

References

Bivona BJ, Park S and Harrison-Bernard LM (2011) Glomerular filtration rate determinations in conscious type II diabetic mice. *Am J Physiol-Renal* **300**:F618-F625.

Brenner BM, Cooper ME, de Zeeuw D, Keane WF, Mitch WE, Parving HH, Remuzzi G, Snapinn SM, Zhang Z, Shahinfar S and Investigators RS (2001) Effects of losartan on renal and cardiovascular outcomes in patients with type 2 diabetes and nephropathy. *N Engl J Med* **345**:861-869.

Cherney DZ, Perkins BA, Soleymanlou N, Maione M, Lai V, Lee A, Fagan NM, Woerle HJ, Johansen OE, Broedl UC and von Eynatten M (2014) Renal hemodynamic effect of sodium-glucose cotransporter 2 inhibition in patients with type 1 diabetes mellitus. *Circulation* **129**:587-597.

Coady MJ, El Tarazi A, Santer R, Bissonnette P, Sasseville LJ, Calado J, Lussier Y, Dumayne C, Bichet DG and Lapointe JY (2017) MAP17 Is a Necessary Activator of Renal Na+/Glucose Cotransporter SGLT2. *Journal of the American Society of Nephrology : JASN* **28**:85-93.

de Zeeuw D, Remuzzi G, Parving HH, Keane WF, Zhang Z, Shahinfar S, Snapinn S, Cooper ME, Mitch WE and Brenner BM (2004) Proteinuria, a target for renoprotection in patients with type 2 diabetic nephropathy: lessons from RENAAL. *Kidney Int* **65**:2309-2320.

Dekkers CCJ, Petrykiv S, Laverman GD, Cherney DZ, Gansevoort RT and Heerspink HJL (2018) Effects of the SGLT-2 inhibitor dapagliflozin on glomerular and tubular injury markers. *Diabetes Obes Metab* **20**:1988-1993.

Ferrannini E, Ramos SJ, Salsali A, Tang W and List JF (2010) Dapagliflozin monotherapy in type 2 diabetic patients with inadequate glycemic control by diet and exercise: a randomized, double-blind, placebo-controlled, phase 3 trial. *Diabetes Care* **33**:2217-2224.

Fioretto P, Del Prato S, Buse JB, Goldenberg R, Giorgino F, Reyner D, Langkilde AM, Sjostrom CD, Sartipy P and Investigators DS (2018) Efficacy and safety of dapagliflozin in patients with type 2 diabetes and moderate renal impairment (chronic kidney disease stage 3A): The DERIVE Study. *Diabetes Obes Metab* **20**:2532-2540.

Fioretto P, Giaccari A and Sesti G (2015) Efficacy and safety of dapagliflozin, a sodium glucose cotransporter 2 (SGLT2) inhibitor, in diabetes mellitus. *Cardiovasc Diabetol* **14**:142.

Flyvbjerg A, Dagnaes-Hansen F, De Vriese AS, Schrijvers BF, Tilton RG and Rasch R (2002) Amelioration of long-term renal changes in obese type 2 diabetic mice by a neutralizing vascular endothelial growth factor antibody. *Diabetes* **51**:3090-3094.

Fu Y, Gerasimova M, Mayoux E, Masuda T and Vallon V (2014) SGLT2 inhibitor empagliflozin increases renal NHE3 phosphorylation in diabetic Akita mice: possible implications for the prevention of glomerular hyperfiltration. *Diabetes* **63**:A132.

Guthrie R (2018) Canagliflozin and cardiovascular and renal events in type 2 diabetes. *Postgrad Med* **130**:149-153.

Hallow KM and Gebremichael Y (2017a) A Quantitative Systems Physiology Model of Renal Function and Blood Pressure Regulation: Application in Salt-Sensitive Hypertension. *CPT Pharmacometrics Syst Pharmacol* **6**:393-400.

Hallow KM and Gebremichael Y (2017b) A quantitative systems physiology model of renal function and blood pressure regulation: Model description. *CPT Pharmacometrics Syst Pharmacol* **6**:383-392.

Hallow KM, Gebremichael Y, Helmlinger G and Vallon V (2017a) Primary proximal tubule hyperreabsorption and impaired tubular transport counterregulation determine glomerular hyperfiltration in diabetes: a modeling analysis. *Am J Physiol Renal Physiol* **312**:F819-F835.

Hallow KM, Greasley PJ, Helmlinger G, Chu L, Heerspink HJL and Boulton DW (2018) Evaluation of renal and cardiovascular protection mechanisms of SGLT2 inhibitors: model-based analysis of clinical data. *Am J Physiol Renal Physiol*. 315(15): F1295-1306.

Hallow KM, Helmlinger G, Greasley PJ, McMurray JJV and Boulton DW (2017b) Why do SGLT2 inhibitors reduce heart failure hospitalization? A differential volume regulation hypothesis. *Diabetes Obes Metab*. 20(3):479-487.

Hallow KM, Lo A, Beh J, Rodrigo M, Ermakov S, Friedman S, de Leon H, Sarkar A, Xiong Y, Sarangapani R, Schmidt H, Webb R and Kondic AG (2014) A model-based approach to investigating the

pathophysiological mechanisms of hypertension and response to antihypertensive therapies: extending the Guyton model. *Am J Physiol Regul Integr Comp Physiol* **306**:R647-662.

Hammon M, Grossmann S, Linz P, Kopp C, Dahlmann A, Garlichs C, Janka R, Cavallaro A, Luft FC, Uder M and Titze J (2015) 23Na Magnetic Resonance Imaging of the Lower Leg of Acute Heart Failure Patients during Diuretic Treatment. *PLoS One* **10**:e0141336.

Heerspink HJ, Johnsson E, Gause-Nilsson I, Cain VA and Sjostrom CD (2016) Dapagliflozin reduces albuminuria in patients with diabetes and hypertension receiving renin-angiotensin blockers. *Diabetes Obes Metab* **18**:590-597.

Holtkamp FA, de Zeeuw D, Thomas MC, Cooper ME, de Graeff PA, Hillege HJ, Parving HH, Brenner BM, Shahinfar S and Lambers Heerspink HJ (2011) An acute fall in estimated glomerular filtration rate during treatment with losartan predicts a slower decrease in long-term renal function. *Kidney Int* **80**:282-287.

Kamei S, Iwamoto M, Kameyama M, Shimoda M, Kinoshita T, Obata A, Kimura T, Hirukawa H, Tatsumi F, Kohara K, Nakanishi S, Mune T, Kaku K and Kaneto H (2018) Effect of Tofogliflozin on Body Composition and Glycemic Control in Japanese Subjects with Type 2 Diabetes Mellitus. *J Diabetes Res* **2018**:6470137.

Kohan DE, Fioretto P, Tang W and List JF (2014) Long-term study of patients with type 2 diabetes and moderate renal impairment shows that dapagliflozin reduces weight and blood pressure but does not improve glycemic control. *Kidney Int* **85**:962-971.

Lambers Heerspink HJ, de Zeeuw D, Wie L, Leslie B and List J (2013) Dapagliflozin a glucose-regulating drug with diuretic properties in subjects with type 2 diabetes. *Diabetes Obes Metab* **15**:853-862.

Lazzara MJ and Deen WM (2007) Model of albumin reabsorption in the proximal tubule. *Am J Physiol-Renal* **292**:F430-F439.

Levine DZ, Iacovitti M and Robertson SJ (2008) Modulation of single-nephron GFR in the db/db mouse model of type 2 diabetes mellitus. II. Effects of renal mass reduction. *Am J Physiol-Reg I* **294**:R1840-R1846.

Lewis EJ, Hunsicker LG, Clarke WR, Berl T, Pohl MA, Lewis JB, Ritz E, Atkins RC, Rohde R, Raz I and Collaborative Study G (2001) Renoprotective effect of the angiotensin-receptor antagonist irbesartan in patients with nephropathy due to type 2 diabetes. *N Engl J Med* **345**:851-860.

List JF, Woo V, Morales E, Tang W and Fiedorek FT (2009) Sodium-glucose cotransport inhibition with dapagliflozin in type 2 diabetes. *Diabetes Care* **32**:650-657.

Mahato HS, Ahlstrom C, Jansson-Lofmark R, Johansson U, Helmlinger G and Hallow KM (2019) Mathematical model of hemodynamic mechanisms and consequences of glomerular hypertension in diabetic mice. *NPJ Syst Biol Appl* **5**:2.

Mann JF, Schmieder RE, McQueen M, Dyal L, Schumacher H, Pogue J, Wang X, Maggioni A, Budaj A, Chaithiraphan S, Dickstein K, Keltai M, Metsarinne K, Oto A, Parkhomenko A, Piegas LS, Svendsen TL, Teo KK, Yusuf S and investigators O (2008) Renal outcomes with telmisartan, ramipril, or both, in people at high vascular risk (the ONTARGET study): a multicentre, randomised, double-blind, controlled trial. *Lancet* **372**:547-553.

Marre M, Puig JG, Kokot F, Fernandez M, Jermendy G, Opie L, Moyseev V, Scheen A, Ionescu-Tirgoviste C, Saldanha MH, Halabe A, Williams B, Mion Junior D, Ruiz M, Hermansen K, Tuomilehto J, Finizola B, Gallois Y, Amouyel P, Ollivier JP and Asmar R (2004) Equivalence of indapamide SR and enalapril on microalbuminuria reduction in hypertensive patients with type 2 diabetes: the NESTOR Study. *J Hypertens* **22**:1613-1622.

Maruyama T, Takashima H, Oguma H, Nakamura Y, Ohno M, Utsunomiya K, Furukawa T, Tei R, Abe M. Canagliflozin Improves Erythropoiesis in Diabetes Patients with Anemia of Chronic Kidney Disease. *Diabetes Technol Ther* **21(12)**:713-720.

McMurray JJV, Solomon SD, Inzucchi SE, Kober L, Kosiborod MN, Martinez FA, Ponikowski P, Sabatine MS, Anand IS, Belohlavek J, Bohm M, Chiang CE, Chopra VK, de Boer RA, Desai AS, Diez M, Drozdz J, Dukat A, Ge J, Howlett JG, Katova T, Kitakaze M, Ljungman CEA, Merkely B, Nicolau JC, O'Meara E, Petrie MC, Vinh PN, Schou M, Tereshchenko S, Verma S, Held C, DeMets DL, Docherty KF, Jhund PS, Bengtsson O, Sjostrand M, Langkilde AM, Committees D-HT and Investigators (2019) Dapagliflozin in Patients with Heart Failure and Reduced Ejection Fraction. *N Engl J Med* **381**:1995-2008.

Mikami Y, Takagi K, Itaya Y, Ono Y, Matsumura H, Takai Y and Seki H (2014) Post-partum recovery course in patients with gestational hypertension and pre-eclampsia. *J Obstet Gynaecol Res* **40**:919-925.

Mosenzon O, Wiviott SD, Cahn A, Rozenberg A, Yanuv I, Goodrich EL, Murphy SA, Heerspink HJL, Zelniker TA, Dwyer JP, Bhatt DL, Leiter LA, McGuire DK, Wilding JPH, Kato ET, Gause-Nilsson IAM, Fredriksson M, Johansson PA, Langkilde AM, Sabatine MS and Raz I (2019) Effects of dapagliflozin on development and progression of kidney disease in patients with type 2 diabetes: an analysis from the DECLARE-TIMI 58 randomised trial. *Lancet Diabetes Endocrinol* **7**:606-617.

Ohara K, Masuda T, Murakami T, Imai T, Yoshizawa H, Nakagawa S, Okada M, Miki A, Myoga A, Sugase T, Sekiguchi C, Miyazawa Y, Maeshima A, Akimoto T, Saito O, Muto S and Nagata D (2019) Effects of the sodium-glucose cotransporter 2 inhibitor dapagliflozin on fluid distribution: A comparison study with furosemide and tolvaptan. **24**:904-911.

Parving HH, Persson F, Lewis JB, Lewis EJ, Hollenberg NK and Investigators AS (2008) Aliskiren combined with losartan in type 2 diabetes and nephropathy. *N Engl J Med* **358**:2433-2446.

Pessoa TD, Campos LC, Carraro-Lacroix L, Girardi AC and Malnic G (2014) Functional role of glucose metabolism, osmotic stress, and sodium-glucose cotransporter isoform-mediated transport on Na+/H+ exchanger isoform 3 activity in the renal proximal tubule. *Journal of the American Society of Nephrology : JASN* **25**:2028-2039.

Petrykiv S, Sjostrom CD, Greasley PJ, Xu J, Persson F and Heerspink HJL (2017) Differential Effects of Dapagliflozin on Cardiovascular Risk Factors at Varying Degrees of Renal Function. *Clin J Am Soc Nephrol* **12**:751-759.

Titze J (2009) Water-free sodium accumulation. *Semin Dial* **22**:253-255.

Titze J (2014) Sodium balance is not just a renal affair. *Curr Opin Nephrol Hypertens* **23**:101-105.

Vallon V and Thomson SC (2017) Targeting renal glucose reabsorption to treat hyperglycaemia: the pleiotropic effects of SGLT2 inhibition. *Diabetologia* **60**:215-225.

van Bommel EJM, Muskiet MHA, van Baar MJB, Tonneijck L, Smits MM, Emanuel AL, Bozovic A, Danser AHJ, Geurts F, Hoorn EJ, Touw DJ, Larsen EL, Poulsen HE, Kramer MHH, Nieuwdorp M, Joles JA and van Raalte DH (2019) The renal hemodynamic effects of the SGLT2 inhibitor dapagliflozin are caused by post-glomerular vasodilatation rather than pre-glomerular vasoconstriction in metformin-treated patients with type 2 diabetes in the randomized, double-blind RED trial. *Kidney Int*.

WADA Y, HAMAMOTO Y, NAKATANI Y, FUJIKAWA J, IWASAKI Y, YOSHIJI S, AIZAWA-ABE M, IWASAKI K, HONJO S and HAMASAKI A (2019) 2343-PUB: Reduction of HbA1c after SGLT2 Inhibitors Correlate with Change in Plasma Osmolarity but Not with Elevation of Hematocrit in Japanese Patients with Type 2 Diabetes. **68**:2343-PUB.

Wang W, Hallow KM and James DA (2016) A Tutorial on RxODE: Simulating Differential Equation Pharmacometric Models in R. *CPT Pharmacometrics Syst Pharmacol* **5**:3-10.

Wanner C, Inzucchi SE, Lachin JM, Fitchett D, von Eynatten M, Mattheus M, Johansen OE, Woerle HJ, Broedl UC, Zinman B and Investigators E-RO (2016) Empagliflozin and Progression of Kidney Disease in Type 2 Diabetes. *N Engl J Med* **375**:323-334.

Wilding JP, Norwood P, T'Joen C, Bastien A, List JF and Fiedorek FT (2009) A study of dapagliflozin in patients with type 2 diabetes receiving high doses of insulin plus insulin sensitizers: applicability of a novel insulin-independent treatment. *Diabetes Care* **32**:1656-1662.

Yamout H, Perkovic V, Davies M, Woo V, de Zeeuw D, Mayer C, Vijapurkar U, Kline I, Usiskin K, Meininger G and Bakris G (2014) Efficacy and safety of canagliflozin in patients with type 2 diabetes and stage 3 nephropathy. *Am J Nephrol* **40**:64-74.

Yavin Y, Mansfield TA, Ptaszynska A, Johnsson K, Parikh S and Johnsson E (2016) Effect of the SGLT2 Inhibitor Dapagliflozin on Potassium Levels in Patients with Type 2 Diabetes Mellitus: A Pooled Analysis. *Diabetes Ther* **7**:125-137.

Zinman B, Wanner C, Lachin JM, Fitchett D, Bluhmki E, Hantel S, Mattheus M, Devins T, Johansen OE, Woerle HJ, Broedl UC, Inzucchi SE and Investigators E-RO (2015) Empagliflozin, Cardiovascular Outcomes, and Mortality in Type 2 Diabetes. *N Engl J Med* **373**:2117-2128.

Funding: This study was funded by AstraZeneca Pharmaceuticals

Figure 1. Base model of renal function. Top Left) The renal vasculature is modeled by a single preafferent resistance vessel flowing into N parallel nephrons. Bottom Left) Glomerular filtration is modeled according to Starling's law. Na^+ and water are reabsorbed at different fractional rates in the proximal tubule, loop of Henle, distal convoluted tubule, and connecting tubule/collecting duct. Glucose and Na^+ reabsorption are coupled through SGLT2 and SGLT1 in the proximal tubule. Top right) The balance between Na^+ and water excretion and intake determine blood volume and Na^+ concentration. Na^+ and water move between the blood and interstitial fluid across a concentration gradient, and Na^+ may be sequestered non-osmotically in a peripheral storage compartment. Blood volume determines venous return and cardiac output, which together with total peripheral resistance determine mean arterial pressure and subsequently renal perfusion pressure, closing the loop. Bottom Right) Multiple regulatory mechanisms, include the RAAS and TGF, provide feedbacks on model variables, in order to maintain or return homeostasis. Adapted from(Hallow et al., 2017a).

Figure 2. A-C) Virtual patient population covers the physiological range of baseline UAER, GFR, and MAP., D-E) After run-in on an ARB (losartan 100mg), baseline distributions are leftward shifted but still cover a wide range.

Figure 3. Effect of virtual patient parameter values on baseline GFR and UAER.

Figure 4. Simulated and observed baseline (top row) and change from baseline (bottom row) in GFR/eGFR and UAER of key diabetic nephropathy clinical trials. Boxes: Simulated median and interquartiles; Gray circles: individual virtual patients; Red: clinical study reported values (RENAAL [27]: UACR is geometric mean ± SD; IDNT [28]: UAER median and interquartile range, no measure of variability reported for change in UAER; NESTOR [29]: UAER geometric mean and interquartile range; AVOID [30]: UAER geometric mean and 95% CI. For all studies, eGFR is mean ± SD. No SD reported for RENAAL change in eGFR).

Figure 5. Baseline characteristics of DAPASALT virtual study arms (T2D preserved GFR n = 250, T2D low GFR n = 250, Non-T2D low GFR n=272). Red bars: Study inclusion exclusion criteria.

Figure 6. DAPASALT T2D with preserved renal function (D-PRF) arm. Simulated time course for change from baseline with 10mg dapagliflozin. Solid line: median, dashed lines: 25-75%, pink bands: 0-100% range of response.

Figure 7. DAPASALT T2D with impaired renal function (D-IRF) arm. Simulated time course for change from baseline with 10mg dapagliflozin. Solid line: median, dashed lines: 25-75%, pink bands: 0-100% range of response.

Figure 8. DAPASALT normoglycemic with impaired renal function (N-IRF) arm. Simulated time course for change from baseline with 10mg dapagliflozin. Solid line: median, dashed lines: 25-75%, pink bands: 0-100% range of response.

Figure 9. Simulated response to daily dosing of 10mg dapagliflozin in DAPASALT study arms. All data are median and interquartile range.

JPET Fast Forward. Published on August 6, 2020 as DOI: 10.1124/jpet.120.000040
This article has not been copyedited and formatted. The final version may differ from this version.

Table 1. Parameters varied to produce virtual patients with varying degrees of diabetes, hypertension, and kidney dysfunction

Mechanism	Parameter	Definition	Units	Range	Median	Equation
Diabetic increase in plasma glucose	C_{glu}	Plasma glucose concentration	mmol/L	7.8-14	9.5	3
Glomerulosclerosis	ΔPerm	Reduction in glomerular permeability	%	0-80	32%	10
Nephron loss	ΔNephrons	Initial value for nephron loss	%	0-95	51%	2
Podocyte damage due to non-hemodynamic factors	$\mu_{other,seiv}$	Permanent increase in sieving coefficient	%	0-50	24.7%	12
Variability in PT protein reabsorption	$RC_{albumin}$	Proxima tubule capacity for protein reabsorption	pg/min/ tubule	1.1 – 2.1	1.68	6
Variability in aldosterone secretion	$Aldo_0$	Normalized aldosterone secretion rate	-	0.5-1.5	1	A60
Variability in renin secretion	$\Delta SEC_{renin,0}$	Change in Renin Secretion Rate	%	-50 - +120	+42%	A52
Variability in sodium intake	$\Phi_{Na,in}$	Sodium intake rate	mEq/day	80-200	159	A30
Increased renal vascular resistance	R_{preaff}	Preafferent arteriole resistance	mmHg-min/L	14-26	20	A1
Increased renal vascular resistance	R_{aff}	Afferent arteriole resistance	mmHg-min/L	10-17	13	A1
Increased PT sodium reabsorption	η_{pt}	PT fractional Na+ reabsorption rate	-	0.6 – 0.84	0.717	13
Increased collecting duct sodium reabsorption	η_{cd}	Collecting duct fractional Na+ reabsorption rate	-	0.8-0.9	0.85	A14
Reduced sensitivity to pressure natriuresis signals	S_{P-N}	Pressure natriuresis sensitivity	-	0-1	0.5	A50
Altered pressure natriuresis setpoint	$RIHP_0$	Renal interstitial hydrostatic pressure setpoint	mmHg	9.6-10	9.8	A50

JPET Fast Forward. Published on August 6, 2020 as DOI: 10.1124/jpet.120.000040
This article has not been copyedited and formatted. The final version may differ from this version.

Table 2. Primary and Secondary Endpoints of the DAPASALT study

Variable	Type	Measure	Timepoints
24 hr Sodium excretion	Primary	Change in mean	Baseline vs. mean of days 2-4
	Secondary		Baseline vs mean of days 12-14
	Secondary		Days 12-14 vs days 15-17
24 hr Sodium excretion 24 hr Sodium excretion 24 hr Systolic blood pressure	Secondary	Change in mean	Baseline vs day 4
24 hr Systolic blood pressure			Baseline vs day 13
24 hr Systolic blood pressure			Day 13 vs day 17
Plasma volume	Secondary	Change in mean	Baseline vs Day 4
			Baseline vs Day 14
			Day 14 vs Day 17
Extracellular Fluid Volume	Secondary	Change in mean	Baseline vs Day 14

JPET Fast Forward. Published on August 6, 2020 as DOI: 10.1124/jpet.120.000040
This article has not been copyedited and formatted. The final version may differ from this version.

Table 3. Prevalence of albuminuria and hypertension in virtual patient population, by renal function status.

Renal function	Microalbuminuria	Macroalbuminuria	Hypertensive
Impaired, GFR < 60 ml/min (n=592)	43.4%	58.0%	83%
Moderate impairment, GFR 60-90 (n=794)	53.4%	46.5%	71.6%
Normal, GFR > 90 ml/min (n=2003)	61.1%	38.9%	68.6%

JPET Fast Forward. Published on August 6, 2020 as DOI: 10.1124/jpet.120.000040
This article has not been copyedited and formatted. The final version may differ from this version.

Figure 1

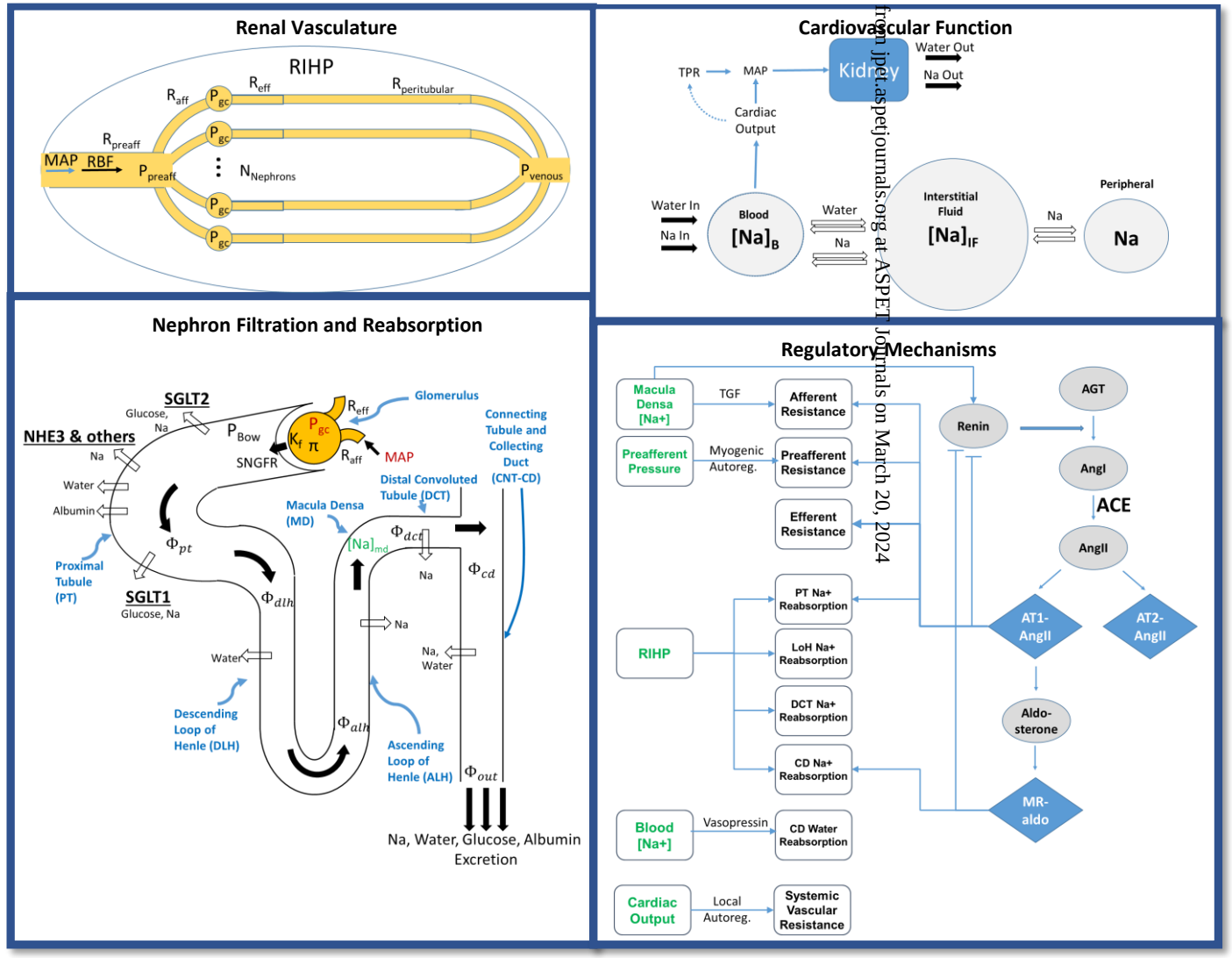

Figure 1

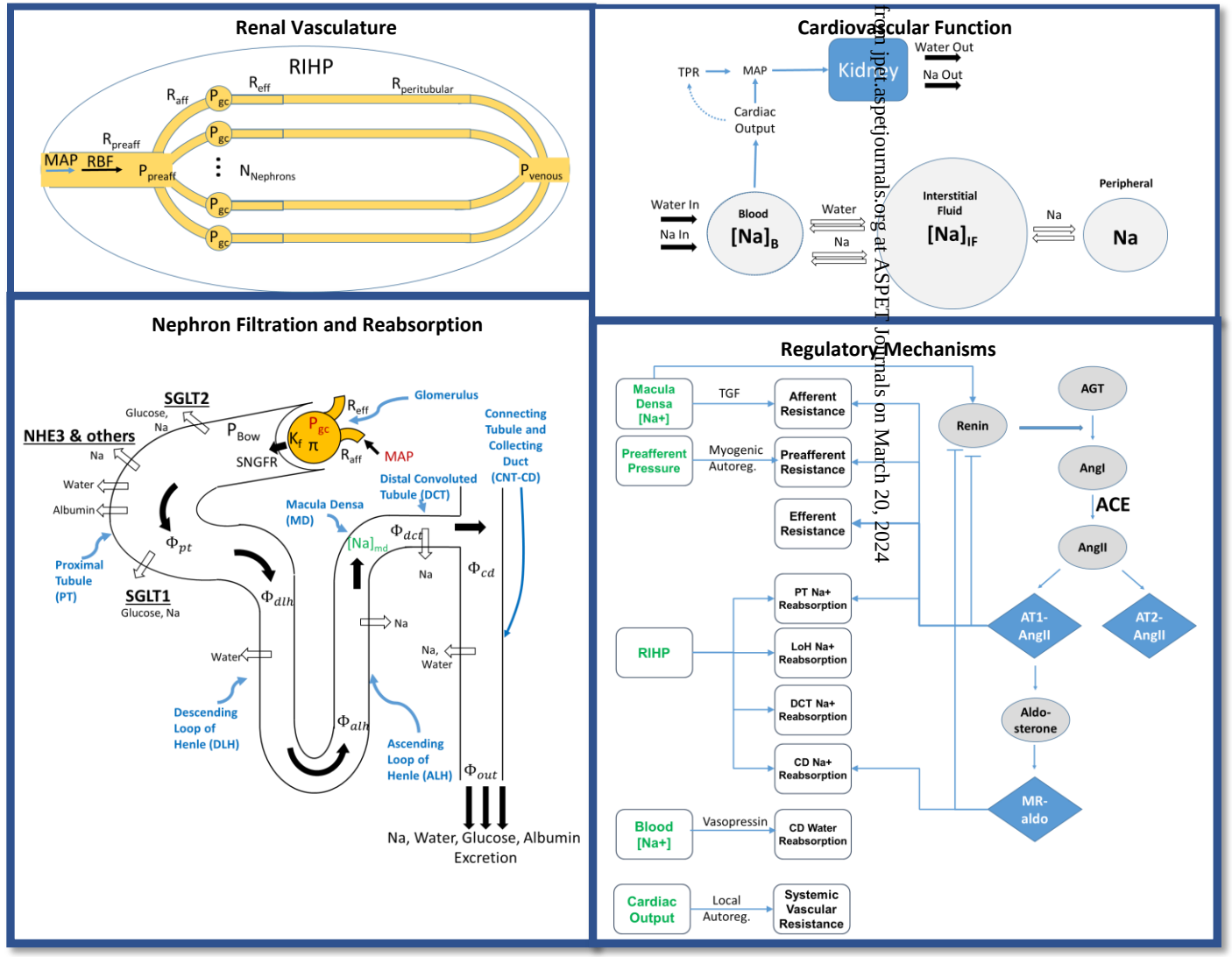

JPET Fast Forward. Published on August 6, 2020 as DOI: 10.1124/jpet.120.000040
This article has not been copyedited and formatted. The final version may differ from this version.

Figure 2

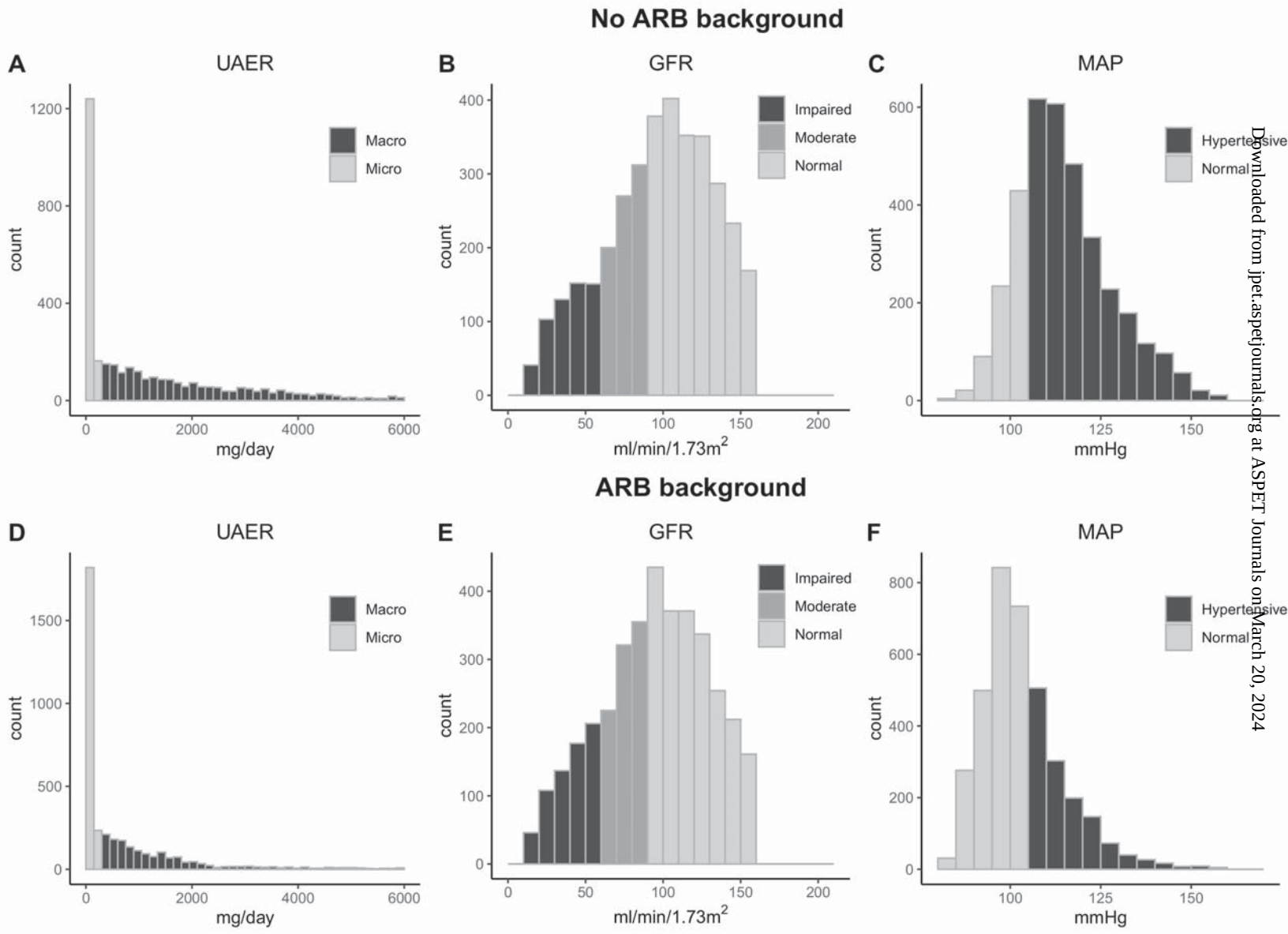

JPET Fast Forward. Published on August 6, 2020 as DOI: 10.1124/jpet.120.000040
This article has not been copyedited and formatted. The final version may differ from this version.

Figure 3

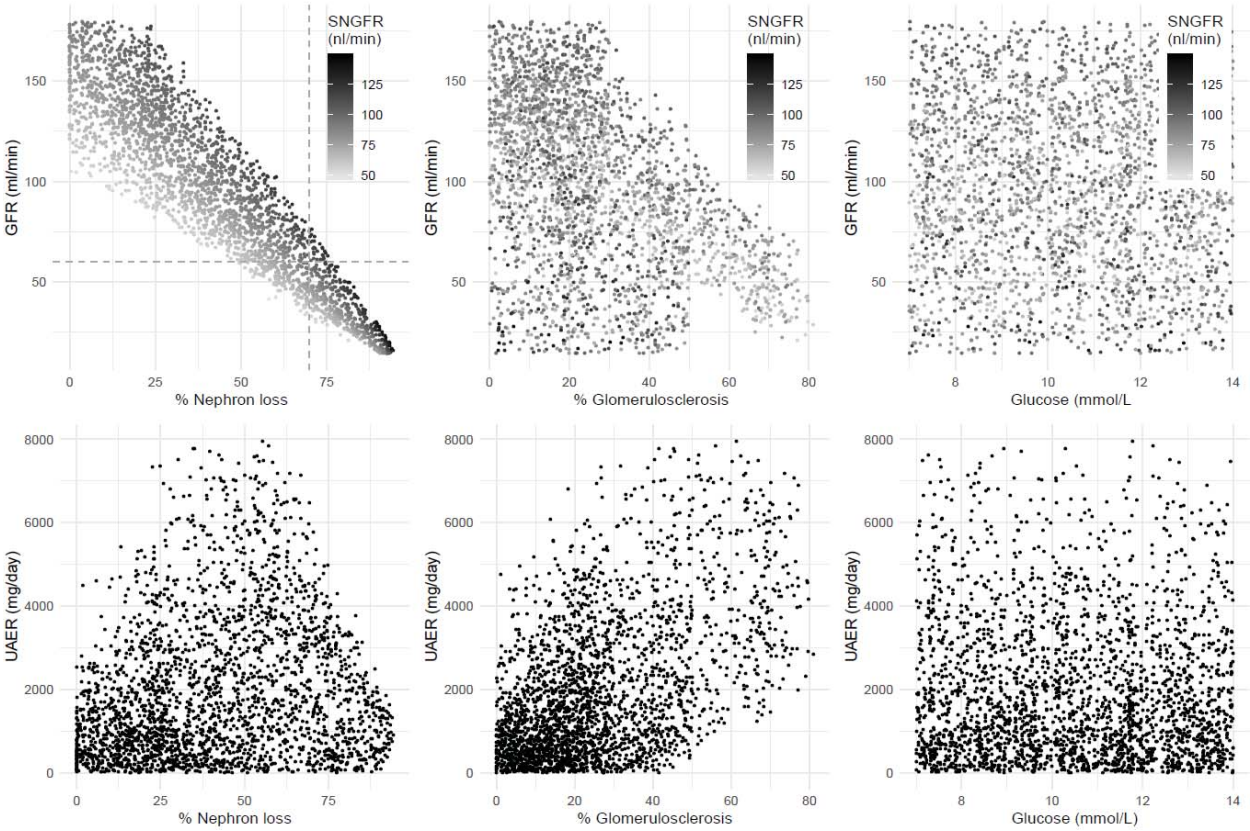

Figure 4

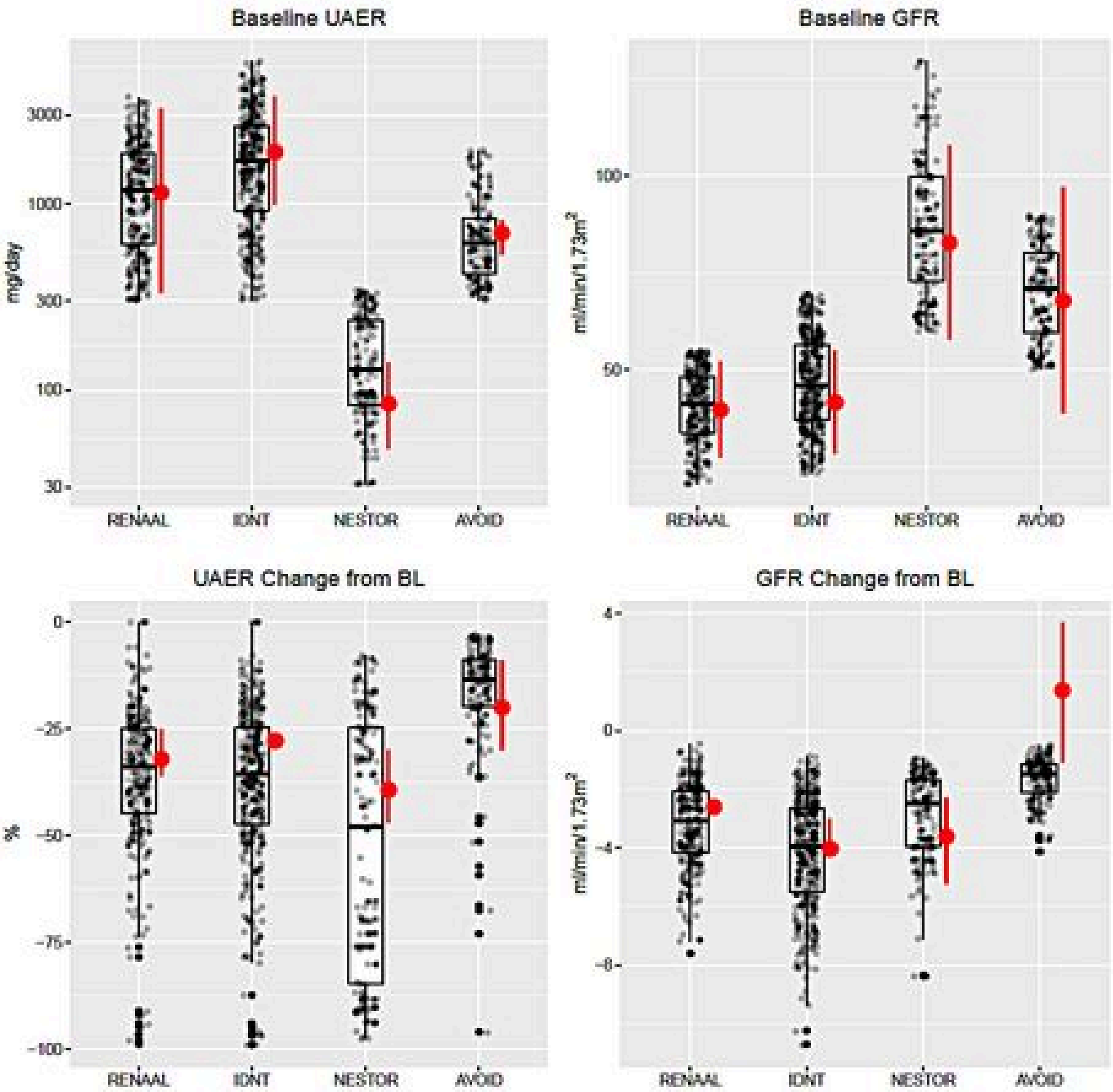
Baseline UAER
mg/day
3000
1000
300
100
30
RENAAL
IDNT
NESTOR
AVOID
Baseline GFR
ml/min/1.73m²
100
50
RENAAL
IDNT
NESTOR
AVOID
UAER Change from BL
%
0
-25
-50
-75
-100
RENAAL
IDNT
NESTOR
AVOID
GFR Change from BL
ml/min/1.73m²
4
0
-4
-8
RENAAL
IDNT
NESTOR
AVOID

JPET Fast Forward. Published on August 6, 2020 as DOI: 10.1124/jpet.120.000040
This article has not been copyedited and formatted. The final version may differ from this version.

Figure 5

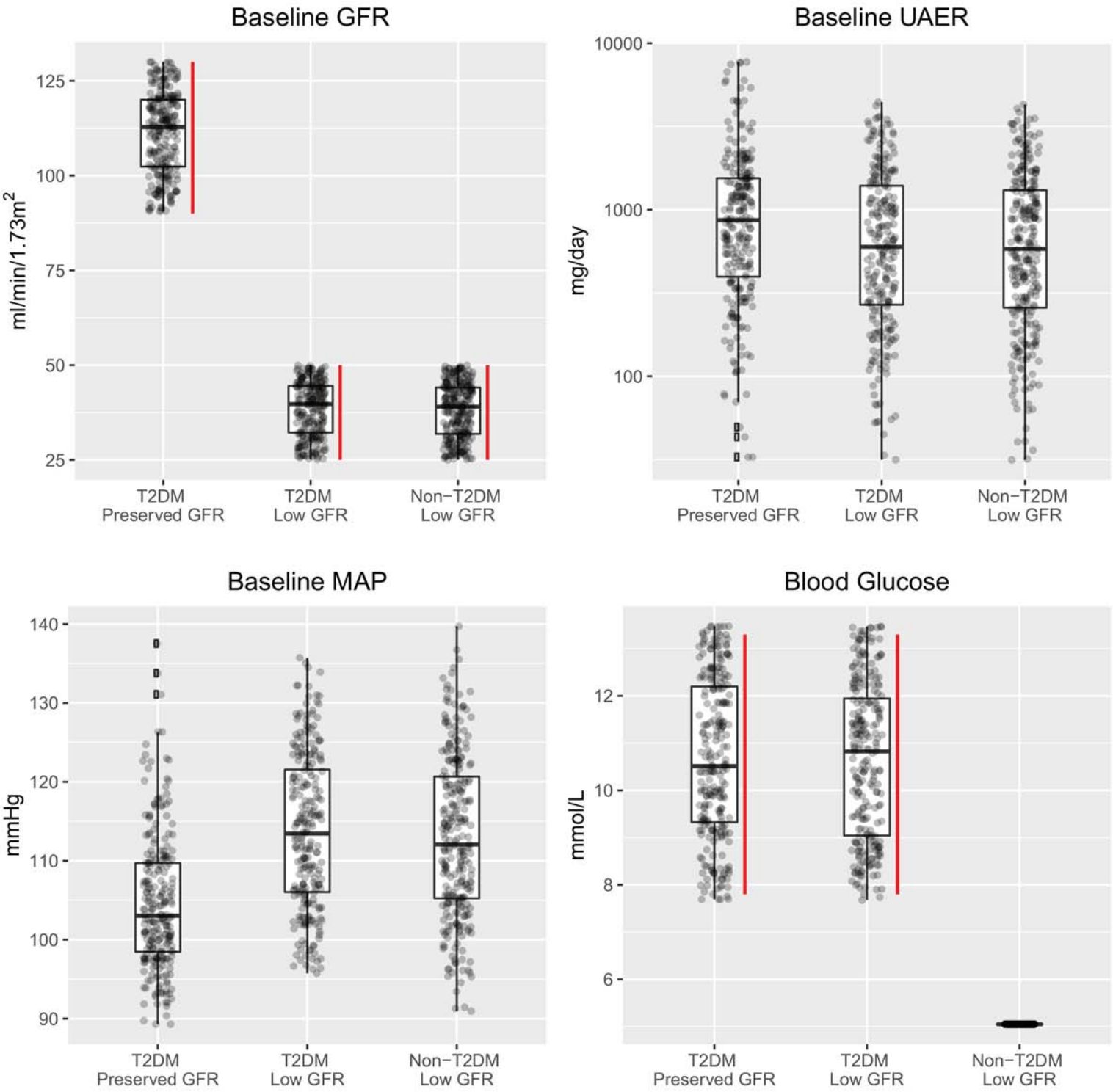

JPET Fast Forward. Published on August 6, 2020 as DOI: 10.1124/jpet.120.000040
This article has not been copyedited and formatted. The final version may differ from this version.

Figure 6

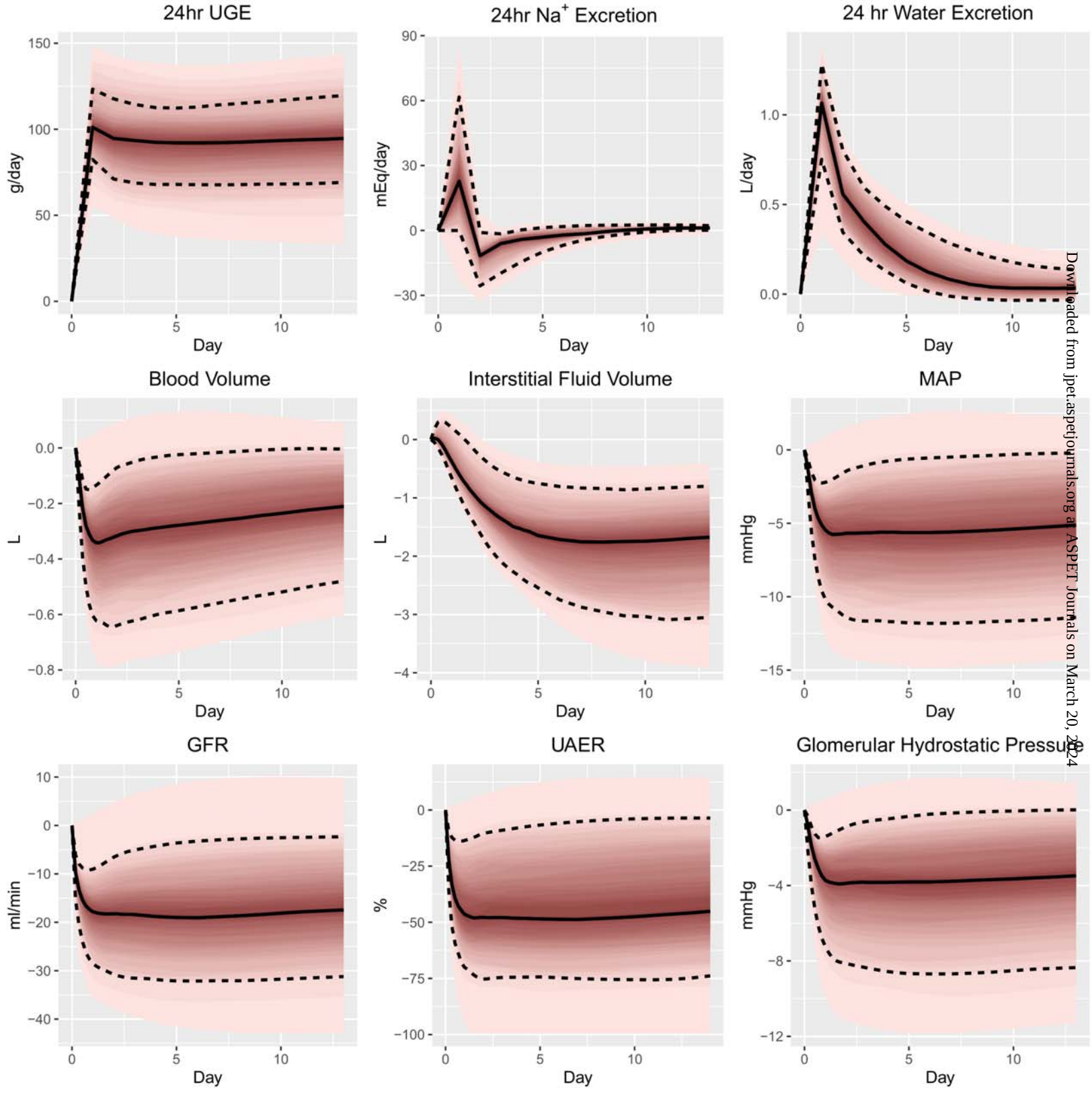

JPET Fast Forward. Published on August 6, 2020 as DOI: 10.1124/jpet.120.000040
This article has not been copyedited and formatted. The final version may differ from this version.

Figure 7

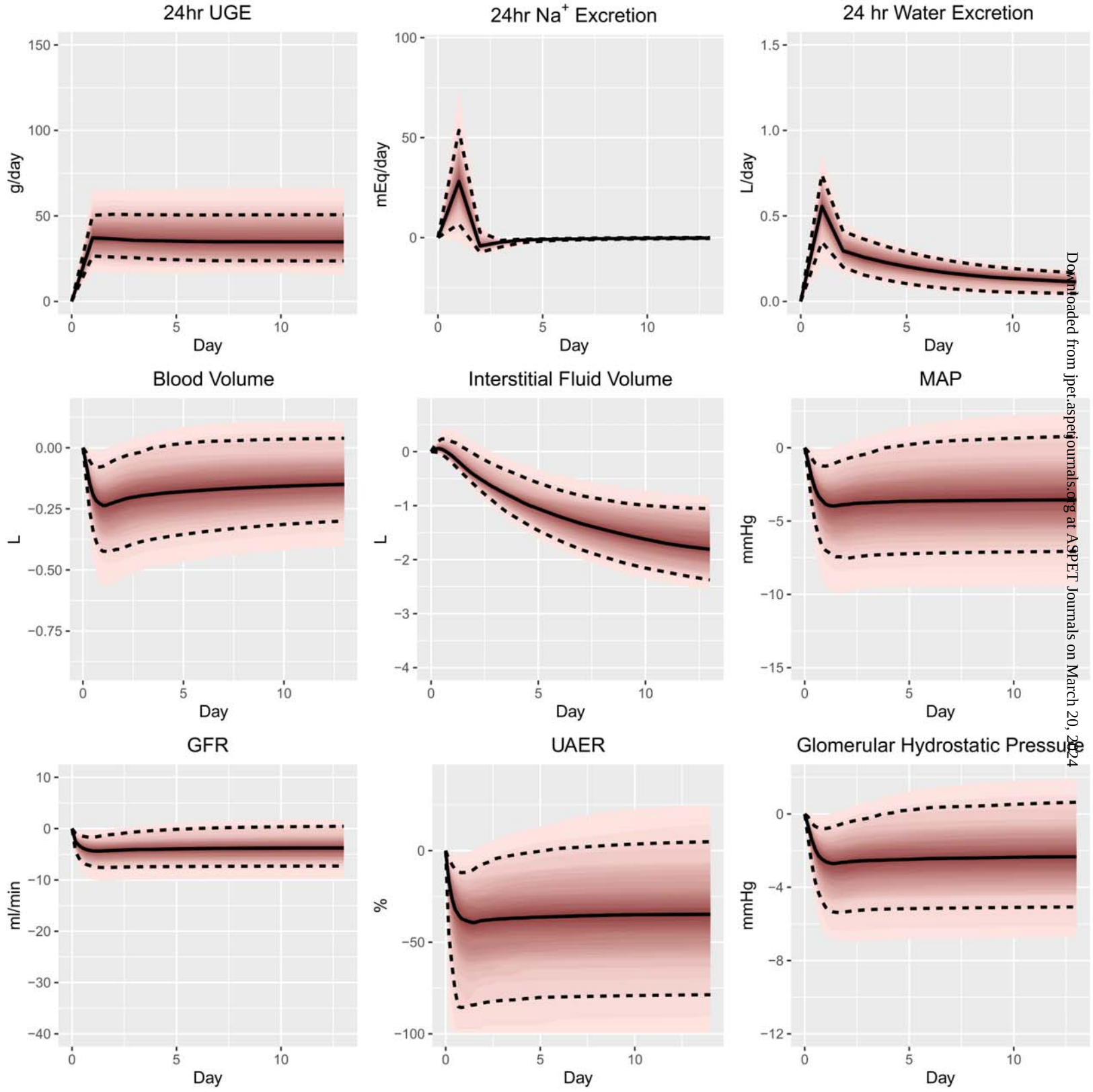

JPET Fast Forward. Published on August 6, 2020 as DOI: 10.1124/jpet.120.000040
This article has not been copyedited and formatted. The final version may differ from this version.

Figure 8

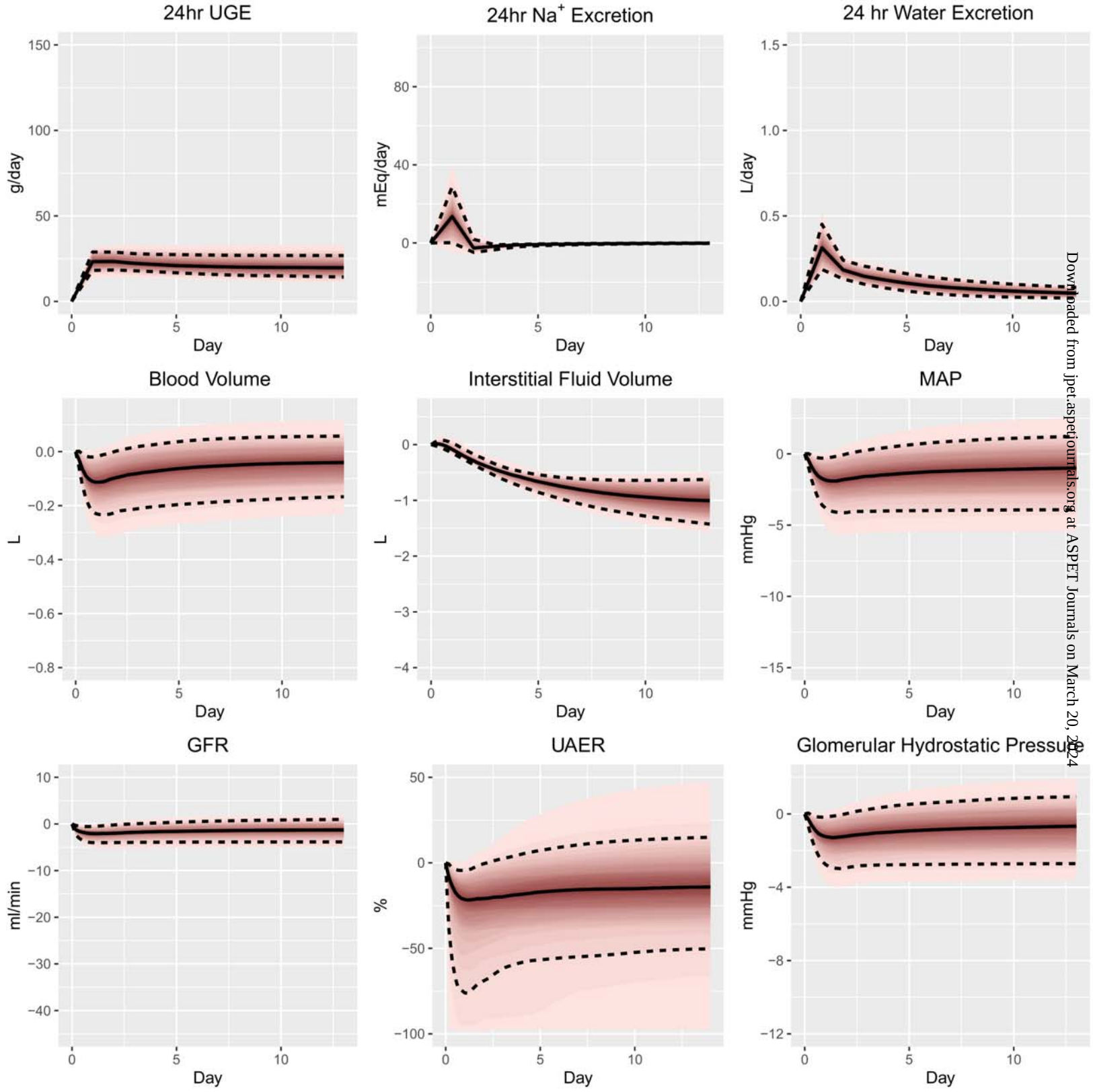

JPET Fast Forward. Published on August 6, 2020 as DOI: 10.1124/jpet.120.000040
This article has not been copyedited and formatted. The final version may differ from this version.

Figure 9

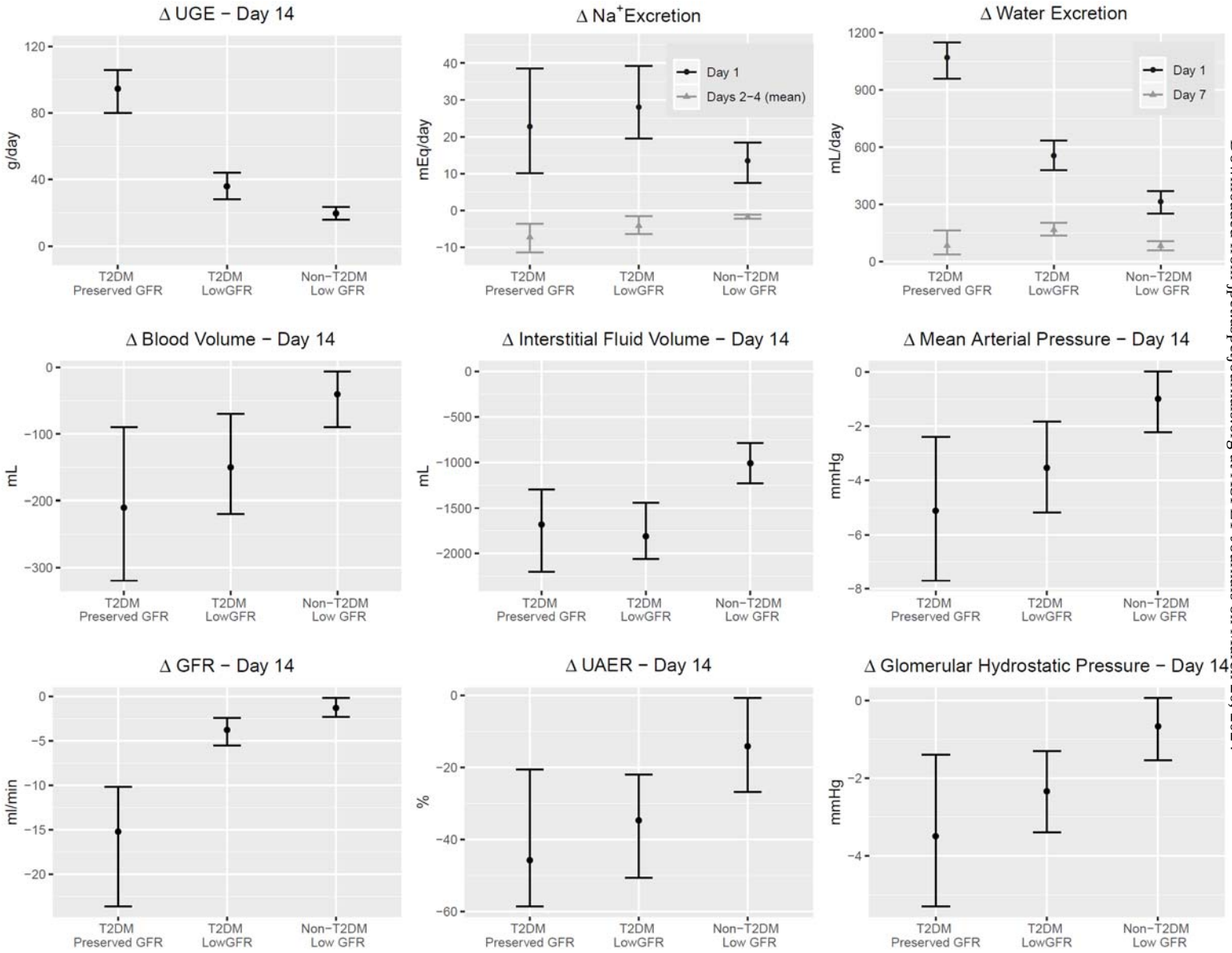

Supplemental Material

Manuscript Title: Renal effects of dapagliflozin in people with and without diabetes with moderate or severe renal dysfunction: prospective modeling of an ongoing clinical trial.

K. Melissa Hallow[1], David W. Boulton[2a], Robert C. Penland[2b], Gabriel Helmlinger[2b], Emily Nieves[1], Daniël H. van Raalte[3], Hiddo L Heerspink[4,5], Peter J. Greasley[6]

1. Department of Chemical, Materials, and Biomedical Engineering, University of Georgia, Athens, GA, USA

2. Clinical Pharmacology and Quantitative Pharmacology, Clinical Pharmacology and Safety Sciences, R&D, AstraZeneca, [a]Gaithersburg, MD, USA, [b]Waltham, MA, USA, [c]Gothenburg, Sweden

3. Diabetes Center, Department of Internal Medicine, Amsterdam University Medical Centers, location VUMC, Amsterdam, The Netherlands

4. Department of Clinical Pharmacy and Pharmacology, University of Groningen, Groningen, Netherlands

5. The George Institute for Global Health, Sydney, Australia

6. Early Clinical Development, Research and Early Development, Cardiovascular, Renal and Metabolism (CVRM) BioPharmaceuticals R&D, AstraZeneca, Gothenburg, Sweden and AstraZeneca R&D, Gothenburg, SE-431 83

Journal of Experimental Pharmacology and Therapeutics

JPET-AR-2020-000040

FULL MODEL EQUATIONS

Renal Vasculature

The glomeruli are modeled in parallel, and in series with the preafferent (interlobar, interlobular, and arcuate arterioles) and peritubular vasculature. Glomerular capillary resistance is assumed negligible. Thus, renal vascular resistance RVR is given by:

$$\mathrm{RVR} = \mathrm{R_{preaff}} + \frac{(R_{aa}+R_{ea})}{N_{nephrons}} + R_{peritubular} \qquad \text{Eq. A1}$$

R_{preaff} and $R_{peritubular}$ are lumped resistances describing the total resistance of preafferent and peritubular vasculatures, respectively, while R_{aa} and R_{ea} are the resistances of a single afferent or efferent arteriole, as determined from Pouiselle's law, based on the arteriole's diameter d, length L, and blood viscosity μ:

$$R_{aa} = \frac{128\mu L_{aa}}{\pi d_{aa}^4}; \quad R_{ea} = \frac{128\mu L_{ea}}{\pi d_{ea}^4} \qquad \text{Eq. A2}$$

$N_{nephrons}$ is the number of nephrons. All nephrons are assumed identical, and the model does not account for spatial heterogeneity.

Renal blood flow (RBF) is a function of the pressure drop across the kidney and RVR, according to Ohm's law:

$$RBF = \frac{MAP - P_{renal-vein}}{RVR} + \frac{GFR\left(\frac{R_{ea}}{N_{nephrons}}\right)}{RVR} \qquad \text{Eq. A3}$$

Renal venous pressure ($P_{renal\text{-}vein}$) is treated as constant. The second term in this equation accounts for lower flow through the efferent arterioles due to GFR. As an approximation, all filtrate is assumed reabsorbed back into the peritubular capillaries, so that peritubular flow is the same as afferent flow.

P_{gc} is determined according to Ohm's law:

$$\mathrm{P_{gc}} = \mathrm{MAP} - \mathrm{RBF} * (\mathrm{R_{preaff}} + \mathrm{R_{aa}}/\mathrm{N_{nephrons}}) \qquad \text{Eq. A4}$$

Determination of MAP, P_{Bow} and $\pi_{go\text{-}avg}$ are described later.

Single nephron glomerular filtration rate (SNGFR) is defined according to Starling's equation, where K_f is the glomerular ultrafiltration coefficient, P_{gc} is glomerular capillary hydrostatic pressure, P_{Bow} is pressure in the Bowman's space, and $\pi_{go\text{-}avg}$ is average glomerular capillary oncotic pressure.

$$SNGFR = K_f \left(P_{gc} - P_{Bow} - \pi_{go-avg} \right) \quad \text{Eq. A5}$$

The total GFR is then the SNGFR multiplied by the number of nephrons:

$$GFR = SNGFR * N_{nephrons} \quad \text{Eq. A6}$$

Glucose filtration, reabsorption, and excretion

Glucose is filtered freely through the glomerulus, so that single nephron filtered glucose load is:

$$\Phi_{glu,filtered} = SNGFR * C_{glu} \quad \text{Eq. A7}$$

where C_{glu} is the plasma glucose concentration.

Glucose reabsorbed in the S1 and S2 segments is given by:

$$\Phi_{glu,reabs.s12} = \min(\Phi_{glu,filtered}, J_{glu,S12} * L_{pt,S12}) \quad \text{Eq. A8}$$

where $J_{glu,S12}$ is the rate of glucose reabsorption per unit length of the S1 and S2 segments together, and $L_{pt,S12}$ is the length of the PT S1 and S2 segments together. Similarly, glucose reabsorbed in the S3 segment is given by:

$$\Phi_{glu,reabs,S3} = \min(\ J_{glu,S3} * L_{pt,S3}, \Phi_{glu,filtered} - \Phi_{glu,reabs,S12}) \quad \text{Eq. A9}$$

Any unreabsorbed glucose then flows through the rest of the tubule and is ultimately excreted, so that the rate of urinary glucose excretion (R_{UGE}) is:

$$R_{UGE} = \Phi_{\mathrm{glu,out-PT}} = \Phi_{glu,filtered} - \Phi_{glu,reabs,S12} - \Phi_{glu,reabs,S3} \qquad \text{Eq. A10}$$

Glucose reabsorption occurs exclusively in the PT through Na^+ glucose cotransporters (SGLT). SGLT2 in the S1 and S2 segments of the PT reabsorbs 90-97% of filtered glucose, while SGLT1 in the S3 segment reabsorbs the remaining 3-10%(*39-43*). At high plasma glucose concentrations, filtered glucose can exceed the kidney's capacity for reabsorption, and the excess glucose is excreted. $J_{glu,S12}$ and $J_{glu,s3}$ represent the number and function of SGLT2 and SGLT1 transporters respectively. The values were determined such that 95% of filtered glucose is reabsorbed in the S1 and S2 segments, while the remaining glucose was reabsorbed in the S3 segment, and so that all glucose is reabsorbed and urinary glucose excretion is zero for blood glucose concentrations up to 9 mmol/l(*44*).

Na^+ filtration and reabsorption in the PT

Similarly to glucose, Na^+ is freely filtered across the glomerulus, so that the single nephron filtered Na^+ load is given by:

$$\Phi_{\mathrm{Na,filtered}} = SNGFR * C_{Na} \qquad \text{Eq.A11}$$

where C_{Na} is the plasma Na^+ concentration.

The rate of Na^+ reabsorption through SGLT2 equals the rate of glucose reabsorption in the S1 and S2 segments, since SGLT2 reabsorb sodium and glucose at a 1:1 molar ratio:

$$\Phi_{\mathrm{Na,reabs-SGLT2}} = \Phi_{glu,reabs,S12} \quad \text{Eq. A12}$$

The rate of Na^+ reabsorption through SGLT1 is twice the rate of glucose reabsorption in the S3 segment, since SGLT1 reabsorb sodium and glucose at a 2:1 molar ratio:

$$\Phi_{\mathrm{Na,reabs-SGLT1}} = 2 * \Phi_{glu,reabs,S3} \quad \text{Eq. A13}$$

Total PT Na^+ reabsorption is then given by:

$$\Phi_{\mathrm{Na,reabs-PT}} = \Phi_{Na,filtered} * \left(\eta_{Na,reabs-PT,NHE3} + \eta_{Na,reabs-PT,other}\right) + \Phi_{\mathrm{Na,reabs-SGLT2}} + \Phi_{\mathrm{Na,reabs-SGLT1}} \quad \text{Eq. A14}$$

where $\eta_{Na,\ reabs\text{-}PT,NHE3}$ and $\eta_{Na,\ reabs\text{-}PT,other}$ are the fractional rates of PT sodium reabsorption through NHE3, and through mechanisms other than SGLT2 and NHE3. Na^+ flow rate out of the PT is then:

$$\Phi_{\mathrm{Na,out-PT}} = \Phi_{Na,filtered} - \Phi_{\mathrm{Na,reabs-PT}} \quad \text{Eq. A15}$$

For the remaining nephron segments, we approximate Na reabsorption in each segment as distributed uniformly along the length, and the rate of reabsorption per unit length is formulated so that the degree of flow-dependence can be varied. For a given segment, the nominal rate of reabsorption per unit length $r_{i,0}$ is given by the following, where η is the baseline fractional rate of reabsorption, $\Phi_{Na,0}(0)$ is the rate delivered to the segment under baseline conditions, and L is the segment length.

$$r_{i,0} = \frac{\eta_i \Phi_{\mathrm{Na,io}}(0)}{L_i} \quad \text{Eq. A16}$$

where i is the ascending LoH (ALH), DCT, or CNT/CD.

The actual rate per unit length r_i is then the nominal rate augmented by a flow-dependent component, as shown in Eq 17. The coefficient B determines the degree of flow-dependence: for B=0, there is no flow dependence; for B=1, changes in reabsorption are directly proportional to flow.

$$r_i = r_{i,0} + \frac{B_i \eta_i \left(\Phi_{\mathrm{Na,i}}(0) - \Phi_{\mathrm{Na,io}}(0)\right)}{L_i} \quad \text{Eq. A17}$$

Na flow along each segment is then:

$$\Phi_{Na,i}(\mathrm{x}) = \Phi_{\mathrm{Na,i}}(0) - \mathrm{r_i} x \quad \text{Eq. A18}$$

$\Phi_{\mathrm{Na,i}}(0)$ is obtained from the Na flow out of the preceding tubule segment.

Water Reabsorption along the tubule

Water reabsorption in the PT is isosmotic. Therefore, water leaving the PT and entering the loop of Henle is given by:

$$\Phi_{water,out-PT} = \Phi_{water,in-DCT} = SNGFR * \frac{\Phi_{osm,filtered}}{\Phi_{osm,out-PT}} \quad \text{Eq. A19}$$

where filtered osmolytes include both sodium and glucose:

$$\Phi_{osm,filtered} = 2 * \Phi_{Na,filtered} + \Phi_{glu,filtered} \quad \text{Eq. A20}$$

$$\Phi_{osm,out-PT} = 2 * \Phi_{Na,out-PT} + \Phi_{glu,out-PT} \quad \text{Eq. A21}$$

In the loop of Henle (LoH), water is reabsorbed in the water permeable descending LoH (DLH) due to the osmotic gradient created by actively pumping sodium out of the water-impermeable ascending limb (ALH). The osmolality along the length of the DLH Osm_{DLH}, which is assumed in equilibrium with the osmolality in the surrounding interstitium Osm_{IS}, is given by:

$$Osm_{DLH}(x) = Osm_{IS}(x) = Osm_{DLH}(0)e^{\frac{r_{ALH}x}{\Phi_{water,in-DCT}Osm_{DLH}(0)}} \quad \text{Eq. A22}$$

Here, x is the distance along the tubule length, and R_{ALH} is the rate of sodium reabsorption per unit length in the ascending loop of Henle (Eq. A17). Water flow through the DLH is then given by:

$$\Phi_{water,DLH}(x) = \frac{\Phi_{water,DLH}(0)Osm_{DLH}(0)}{Osm_{DLH}(x)} \quad \text{Eq. A23}$$

The ALH and the distal convoluted tubule (DCT) are modeled as impermeable to water, so that the flow through these segments equals the flow out of the DLH:

$$\Phi_{water,ALH}(x) = \Phi_{water,DCT}(x) = \Phi_{water,DLH}(L) \quad \text{Eq. A24}$$

In the collecting duct (CD), water reabsorption is driven by the osmotic gradient between the CD tubular fluid and the interstitium, and is modulated by vasopressin, as described later:

$$\Phi_{\text{water,reabs}-\text{CD}} = \mu_{vasopressin}\Phi_{\text{water,CD}}(0) * \left(1 - \frac{Osm_{CD}(L)}{Osm_{IS}(L)}\right) \quad \text{Eq. A25}$$

Where the osmolality in the CD $Osm_{CD}(L)$ accounts for sodium reabsorbed in the collecting duct:

$$Osm_{CD}(L) = \frac{\Phi_{\text{osm,cd}}(0) - 2*\left(\Phi_{\text{Na,cd}}(0) - \Phi_{\text{Na,cd}}(L)\right)}{\Phi_{\text{water,CD}}(0)} \quad \text{Eq. A26}$$

Then, single nephron water excretion rate is given by:

$$\Phi_{\text{water,CD}}(L) = \Phi_{\text{water,CD}}(0) - \Phi_{\text{water,reabs}-\text{CD}} \quad \text{Eq. A27}$$

And urine flow rate is then:

$$\Phi_{\text{urine}} = \text{SNGFR} * \Phi_{\text{water,CD}}(L) \quad \text{Eq. A28}$$

Whole Body Sodium and Water Balance and Peripheral Sodium Storage

We incorporated that three compartment model of volume homeostasis into the renal physiology model, to allow evaluation of the potential role of peripheral sodium storage in the renal response to dapagliflozin. Titze et al have demonstrated dynamic changes in non-osmotically stored sodium in peripheral tissues (Hammon et al. 2015), and we have previously shown that this mechanism is necessary in order explain constant plasma Na+ concentration observed with electrolyte-free water clearance with SGLT2 inhibition (Hallow et al., 2017). Parameters for this portion of the model are given in Table S1. Sodium and water are assumed to move freely between the blood and interstitial fluid. Water and sodium intake rates were assumed constant. Then blood volume (V_b) and blood sodium (Na_{blood}) are the balance between intake and excretion of water and sodium respectively, and the intercompartmental transfer.

$$\frac{d}{dt}(V_b) = Water_{in} - Water_{out} + Q_{water}([Na]_{blood} - [Na]_{IF}) \quad \text{Eq.A29}$$

$$\frac{d}{dt}(Na_{blood}) = \Phi_{\text{Na,intake}} - \Phi_{\text{Na,excretion}} + Q_{Na}([Na]_{IF} - [Na]_{blood}) \quad \text{Eq. A30}$$

Sodium concentrations in the blood and interstitial compartments are assumed to equilibrate quickly. Change in interstitial fluid volume (IFV) is a function of intercompartmental water transfer.

$$\frac{d}{dt}(IFV) = Q_{water}([Na]_{IF} - [Na]_{blood}) \quad \text{Eq. A31}$$

When interstitial sodium concentration $[Na]_{IF}$ exceeds the normal equilibrium level $[Na]_{IF,ref}$, Na+ moves out of the interstitium and is sequestered in the peripheral Na+ compartment, at a rate of $\Phi_{Na,stored}$, where it is osmotically inactive. Thus, the change interstitial fluid sodium depends on intercompartmental transfer and peripheral storage. Sodium cannot be stored indefinitely, and thus there is a limit Nastored,max on how much sodium can be stored. The peripheral sodium compartment can be effectively removed from the model by setting $Q_{Na,stored}$ to zero.

$$\Phi_{\mathrm{Na,stored}} = Q_{Na,stored} * \frac{(Na_{stored,max} - Na_{stored})}{Na_{stored,max}} \left([Na]_{JF} - [Na]_{IF,ref}\right) \quad \text{Eq. A32}$$

$$\frac{d}{dt}(Na_{stored}) = \Phi_{\mathrm{Na,stored}} \quad \text{Eq. A33}$$

$$\frac{d}{dt}(Na_{IF}) = Q_{Na}([Na]_{blood} - [Na]_{IF}) - \Phi_{\mathrm{Na,stored}} \quad \text{Eq. A34}$$

Blood and IF sodium concentrations are then given by:

$$[Na]_{blood} = \frac{Na_{blood}}{V_B} \quad \text{Eq. A35}$$

$$[Na]_{IF} = \frac{Na_{IF}}{IFV} \quad \text{Eq. A36}$$

Tubular Hydrostatic Pressure

Hydrostatic pressure in the Bowman's space is a key factor affecting GFR, and this pressure is influenced by both morphology and flow rates through the tubule. Changes in Na and water reabsorption along the nephron, which can occur either due to disease or treatments, can alter GFR by altering tubular pressures. Thus dynamically modeling tubular pressures can be critical to understanding GFR changes.

Adapting from Jensen et al(16), tubular flow rates described in the main text can be used to determine tubular pressure. The change in intratubular pressure dP^* over a length of tubule dx can be defined according to Poiseuille's law as:

$$dP^* = -\frac{128\mu}{\pi D^4}\Phi_{water}(x)dx \qquad \text{Eq. A37}$$

Eq. 36 describes the relationship between transtubular pressure P and tubular diameter D, where D_c is the diameter at control pressure P_c, and β is the exponent of tubular distensibility.

$$\frac{D}{D_c} = \left(\frac{P}{P_c}\right)^{\beta} \qquad \text{Eq. A38}$$

Substituting and assuming uniform interstitial pressure throughout the kidney, we obtain:

$$dP = -\frac{128\eta}{\pi D_c^4}\left(\frac{P_c}{P}\right)^{4\beta}\Phi_{water}(x)\,dx \qquad \text{Eq A39}$$

Integrating over a tubule segment length, we obtain inlet pressure as a function of the outlet pressure and the flow rate:

$$P_{in} = \left[P_{out}^{4\beta+1} + \frac{(4\beta+1)128\eta P_c^{4\beta}}{\pi D_c^4}\int_0^L \Phi_{water}(x)dx\right]^{\frac{1}{4\beta+1}} \qquad \text{Eq A40}$$

The pressure calculated at the inlet to the PT is used as P_{Bow} in Eq. A5 above.

Because the diameter of the CNT/CD changes as nephrons coalescence, calculating pressure along this segment is challenging. Under normal conditions, pressure drops 5-7mmHg across the CNT/CD. Thus, an effective control diameter was calculated to give this degree of pressure drop under baseline conditions.

Glomerular Capillary Oncotic Pressure

The glomerular capillary oncotic pressure is calculated using the Landis Pappenheimer equation, where C_{prot} is the concentration of protein at the point of interest.

$$\pi = 1.629 * C_{prot} + 0.2935 * C_{prot}^2 \quad \text{Eq. A41}$$

Plasma protein ($C_{prot\text{-}plasma}$) is assumed constant. Protein concentration at the distal end of the glomerulus ($C_{prot\text{-}glom\text{-}out}$) is determined as:

$$C_{prot-glom-out} = C_{prot-plasma} * \frac{RBF}{RBF-GFR} \quad \text{Eq. A42}$$

Protein concentration is assumed to be varying linearly along the capillary length, and thus the oncotic pressure π_{go-avg} is calculated using the average of the plasma protein concentration and protein concentration at the distal end of the glomerulus.

The model does not account for filtration equilibrium, which may occur in some species.

Regulatory Mechanisms

Multiple control mechanisms act on the system to allow simultaneous control of C_{na}, CO, MAP, glomerular pressure, and RBF. For each control mechanism, the feedback signal μ is modeled by one of two functional forms. The choice of functional form is determined by whether a steady state error is allowed in the controlled variable X. When a steady state error is not allowed (i.e. X always eventually returns to the setpoint X_0), the effect is defined by a proportional-integral (PI) controller. The initial feedback signal is proportional to the magnitude of the error ($X\text{-}X_0$), with gain G. But the feedback continues to grow over time as long as any error exists, until the error returns to zero. The integral gain K_i determines the speed of return to steady-state.

$$\mu = 1 + G * ((X - X_0) + K_i * \int (X - X_0) dt) \quad \text{Eq. A43}$$

All other mechanisms, for which the controlled variable can deviate from the setpoint at steady-state, are described by a logistic equation that produces a saturating response characteristic of biological signals:

$$\mu = 1 + S * \left(\frac{1}{1+\exp\left(\frac{X-X_0}{m}\right)} - 0.5 \right) \quad \text{Eq. A44}$$

Here, m defines the slope of the response around the operating point, and S is the maximal response as X goes to $\pm\infty$.

Control of plasma Na concentration by vasopressin

Changes in plasma osmolality are sensed via osmoreceptors, stimulating vasopressin secretion, which exerts control of water reabsorption in the CNT/CD. To insure that blood sodium concentration C_{Na} is maintained at its setpoint $C_{Na,0}$ at steady state, this process is modeled by a PI controller:

$$\mu_{vasopressin} = 1 + G_{Na-vp} * \left(C_{Na} + K_{i-vp} * \int \left(C_{Na} - C_{Na,0} \right) dt \right) \quad \text{Eq. A45}$$

The parameters $G_{Na\text{-}vp}$ and $K_{i\text{-}vp}$ are gains of proportional and integral control, respectively.

Tubular Pressure Natriuresis

For homeostasis, Na excretion over the long-term must exactly match Na intake (the principle of Na balance). Any steady-state Na imbalance would lead to continuous volume retention or loss– an untenable situation. Pressure-natriuresis(2), wherein changes in renal perfusion pressure (RPP) induce changes in Na excretion, insures that Na balance is maintained. It may be partially achieved through neurohumoral mechanisms including the RAAS, but there is also an intrinsic pressure-mediated effect on tubular Na reabsorption, where renal interstitial hydrostatic pressure (RIHP) is believed to be the driving signal. RIHP is a function of peritubular capillary pressure, and is calculated according to Ohm's law:

$$P_{peritubular} = MAP - RBF * \left(R_{preaff} + \frac{R_{aff}+R_{eff}}{N_{nephrons}} \right) \quad \text{Eq. A46}$$

As a simplification, we assume an increase in peritubular pressure will generate a proportional increase in RIHP. Since the kidney is encapsulated, we assume interstitial pressure equilibrates and changes in one

region are transduced across the kidney. The relationship between RIHP and fractional Na reabsorption rate of each tubular segment is then modeled as:

$$\eta_{\mathrm{i-sodreab}} = \eta_{\mathrm{i-sodreab,0}} * \left(1 + S_{\mathrm{P-N,i}} * \left(\frac{1}{1+\exp(\mathrm{RIHP}-RIHP_0)} - 0.5\right)\right) \quad \text{Eq. A47}$$

where i = PT, LoH, DCT, or CNT/CD. $\eta_{i-sodreab,0}$ is the nominal fractional rate of reabsorption for that tubule segment. $RIHP_0$ defines the setpoint pressure and is determined from RIHP at baseline for normal Na intake. $S_{P\text{-}N,i}$ defines the maximal signal as RIHP goes to ∞.

Control of Cardiac Output

CO, which describes total blood flow to body tissues, returns to normal over days to weeks following a perturbation (38). CO regulation is a complex phenomenon that occurs over multiple time scales, but we focus only on long-term control (days to weeks), which is thought to be achieved through whole-body autoregulation - the intrinsic ability of organs to adjust their resistance to maintain constant flow(38). The total effect of local autoregulation of all organs is that TPR is adjusted to maintain CO at a constant resting level. The feedback between CO and TPR is modeled with a PI controller, such that CO is controlled to its steady-state setpoint CO_0.

$$\mathrm{TPR} = \mathrm{TPR}_0 * \left(1 + G_{\mathrm{CO-tpr}} * \left(\mathrm{CO} + K_{\mathrm{i-tpr}} * \int(\mathrm{CO} - \mathrm{CO}_0)\mathrm{dt}\right)\right) \quad \text{Eq. A48}$$

Control of Macula Densa Sodium Concentration by Tubuloglomerular Feedback

Tubuloglomerular feedback (TGF) helps stabilize tubular flow by sensing Na concentration in the the macula densa, which sits between the LoH and DCT, and providing a feedback signal to inversely change afferent arteriole diameter. The TGF effect is defined as:

$$\mu_{TGF} = 1 + S_{TGF} * \left(\frac{1}{1+\exp\left(\frac{C_{Na,MD,0} - C_{Na,MD}}{m_{TGF}}\right)} - 0.5 \right) \quad \text{Eq. A49}$$

The basal afferent arteriole resistance Raa is then multiplied by μ_{TGF} to obtain the ambient afferent arteriolar resistance. The setpoint $C_{Na,MD,0}$ is the Na concentration out of the LoH and into the DCT in the baseline state at normal Na intake.

Myogenic Autoregulation of Glomerular Pressure

Glomerular hydrostatic pressure is normally tightly autoregulated, and changes very little in response to large changes in blood pressure. This autoregulation is in part through myogenic autoregulation of the preglomerular arterioles. While the pressure drop and thus myogenic response varies along the arteriole length, we make the simplifying assumption that the preafferent vasculature responds to control pressure at the distal end.

$$\mu_{autoreg} = 1 + S_{autoreg} * \left(\frac{1}{1+\exp\left(\frac{P_{preafferent} - P_{preafferent,0}}{m_{autoreg}}\right)} - 0.5 \right) \quad \text{Eq. A50}$$

Pressure at the distal end of the preafferent vasculature is given by:

$$P_{preafferent} = MAP - RBF * R_{preaff} \quad \text{Eq. A51}$$

The basal preafferent arteriole resistance R_{preaff} is then multiplied by $\mu_{autoreg}$ to obtain the ambient preafferent arteriolar resistance.

Renin-Angiotensin-Aldosterone System Submodel

Renin is secreted at a nominal rate $SEC_{ren,0}$ modulated by macula densa sodium flow, as well as by a strong negative feedback from Angiotensin II bound to the AT1 receptor.

$$SEC_{renin} = \mu_{md-renin} * \mu_{AT1} * \mu_{rsna} * SEC_{renin,0}$$ Eq. A52

The macula densa releases renin in response to reduced sodium flow:

$$\mu_{md-renin} = e^{-A_{md-ren}(\phi_{Na,md} - \phi_{Na,md,0})}$$ Eq. A53

We have found that the inhibitory effect of AT1-bound AngII on renin secretion can be well described by the following relationship:

$$\mu_{AT1} = \mathrm{A}_{\mathrm{AT1,ren}} \left(\frac{\mathrm{AT1-bound-AngII}}{\mathrm{AT1-bound-AngII_0}} \right)$$ Eq. A54

Renal sympathetic nerve activity is assumed to exert a linear effect on renin secretion. Renin secretion may also be controlled by baroreceptors in the afferent arteriole. However, it is difficult to distinguish between the effects of macula densa sodium flow and preafferent pressure in most experiments, since these variables move in the same direction. As a simplifying assumption, and because have previously found that is provides a better fit to available data (results not published), we neglected the baroreceptor effect and implicitly assume that it is accounted for by the effect of macula-densa sodium flow.

Plasma renin concentration (PRC) is then given by:

$$\frac{d(PRC)}{dt} = SEC_{renin} - K_{d,renin} * PRC$$ Eq. A55

Where $K_{d,renin}$ is the renin degradation rate. PRA can be related to PRC by the conversion factor 0.06 (ng/ml/hr)/(pg/ml).

Angiotensin I is formed by PRA, assuming that its precursor angiotensinogen is available in excess and the plasma renin activity (PRA) is the rate-limiting step. AngI is also converted to AngII by the enzymes ACE and chymase, and is degraded at a rate of $K_{d,AngI}$.

$$\frac{d(AngI)}{dt} = PRA - (ACE + Chymase) * AngI - K_{d,AngI} AngI$$ Eq. A56

Angiotensin II is formed from the action of ACE and chymase on AngI, can be eliminated by binding to either the AT1 or AT2 receptors at the rate K_{AT1} and K_{AT2} respective, and is degraded at a rate of Kd,AngII.

$$\frac{d(AngII)}{dt} = (ACE + Chymase) * AngI - (K_{AT1} + K_{AT2}) * AngII - K_{d,AngII} Ang\text{II} \quad \text{Eq. A57}$$

The complex of Angiotensin II bound to the AT1 receptor is the physiologically active entity within the pathway, and is given by:

$$\frac{d\left(AT1_{bound_{AngII}}\right)}{dt} = (K_{AT1}) * AngII - K_{d,AT1} AT1\_bound\_AngII \quad \text{Eq. A58}$$

AT1-bound AngII has multiple physiologic effects, including constriction of the efferent, as well and preglomerular, afferent, and systemic vasculature, sodium retention in the PT, and aldosterone secretion. Each effect is modeled as:

$$\mu_{AT1,i} = 1 + S_{AT1,i} * \left(\frac{1}{1+\exp\left(\frac{AT1-bound_{AngII_0} - AT1-bound\_AngII}{m_{AT1,i}}\right)} - 0.5 \right)$$

Eq. A59

where i represents the effect on efferent, afferent, preafferent, or systemic resistance, PT sodium reabsorption, or aldosterone secretion.

Aldosterone is the second physiologically active entity in the RAAS pathway, acting by binding to mineralocorticoid receptors (MR) in the CNT/CD and DCT to stimulate sodium reabsorption. MR-bound aldosterone is modeled as the nominal concentration Aldo,0 modulated by the effect of AT1-bound AngII, and the normalized availability of MR receptors (1 in the absence of an MR antagonist).

$$MR - bound\_Aldo = Aldo_0 * \mu_{AT1} * MR \quad \text{Eq. A60}$$

The effects of MR-bound aldosterone on CNT/CD and DCT sodium reabsorption are modeled as:

$$\mu_{aldo,i} = 1 + S_{aldo,i} * \left(\frac{1}{1+exp\left(\frac{MR-bound\ Aldo_0 - MR-bound\ Aldo}{m_{aldo,i}}\right)} - 0.5 \right) \quad \text{Eq. A61}$$

Where i is the CNT/CD or DCT.

Cardiac Model

The ventricular mechanics portion of the model was adapted from a previously published model by Arts, Bovendeerd, and colleagues (1, 6). Many equations were used verbatim from these previous papers. We repeat those equations here for the reader's convenience, but refer the reader to the original publication for more complete explanation. Here we present equations for the left ventricle; analogous equations were used for the right ventricle.

The volume of blood inside the left ventricle chamber V_{lv} is given by:

$$\frac{d(V_{lv})}{dt} = Q_{mitral} - Q_{aorta} \qquad \text{Eq. A62}$$

where Q_{mitral} and Q_{aorta} are blood flow rates through the mitral and aortic valves, respectively, as described later. Bovendeerd et al showed that left ventricular pressure P_{lv} can be related to LV volume V_{lv} and LV wall volume V_w by the following (Ref 6, Eq. 7):

$$P_{lv} = \frac{1}{3}\left(\sigma_f - 2\sigma_{m,r}\right)\ln\left(1 + \frac{V_w}{V_{lv}}\right) \qquad \text{Eq. A63}$$

Here σ_f and $\sigma_{m,r}$ are mechanical stresses in the myocardium along the longitudinal fiber the radial direction respectively. σ_f is comprised of the sum of the passive stress along the fiber $\sigma_{m,f}$ and active fiber stress σ_a. The passive stress along the fiber is a function of the longitudinal stretch along the fiber λ_f and the myocardial longitudinal stiffness c_f (Ref 6, Eq. 14).

$$\sigma_{m,f}\left(\lambda_f\right) = \begin{cases} \sigma_{f0}\left(e^{c_f(\lambda_f - 1)} - 1\right) & \lambda_f \geq 1 \\ 0 & \lambda_f < 1 \end{cases} \qquad \text{Eq. A64}$$

And mean passive radial stress is a function of the radial stretch λ_r and the myocardial radial stiffness c_r (Ref 6, Eq. 15).

$$\sigma_{m,r}(\lambda_r) = \begin{Bmatrix} \sigma_{r0}\left(e^{c_r(\lambda_r - 1)} - 1\right) \\ 0 \end{Bmatrix} \begin{matrix} \lambda_r \geq 1 \\ \lambda_r < 1 \end{matrix} \quad \text{Eq. A65}$$

As shown by Bovendeerd et al, the longitudinal stretch λ_f is related to chamber blood volume and wall volume by (Ref 6, Eq. 8):

$$\lambda_f = \left(\frac{V_{lv} + \frac{1}{3}V_w}{V_{lv,cavity} + \frac{1}{3}V_w} \right)^{\frac{1}{3}} \quad \text{Eq. A66}$$

$V_{lv,cavity}$ is the chamber volume at zero transmural pressure.

The radial stretch λ_r is given by (Ref 6, Eq. 9):

$$\lambda_r = \lambda_f^{-2} \quad \text{Eq. A67}$$

where C_f and C_r are the stiffness of the myocardial tissue in the longitudinal and radial directions, respectively.

LV active stress is a function of contractility (c), sarcomere length l_s, sarcomere shortening velocity V_s, and time elapsed since beginning of contraction (t_a). These equations were taken exactly as shown in Ref 6, Eq. 10 - 13.

Table S1. Baseline Renal Model Parameters

Parameter	Definition	Value	Units

β	Tubular compliance	0.2	-
$\eta_{Na,\ CNT\text{-}CD}$	Fractional rate of CNT/CD Na+ reabsorption	0.827*	-
$\eta_{Na,\ DCT}$	Fractional rate of DCT Na+ reabsorption	0.5	-
$\eta_{Na,\ ALH}$	Fractional rate of PT Na+ reabsorption through PT NHE3	0.8	-
$\eta_{Na,\ reabs\text{-}PT,NHE3}$	Fractional rate of PT Na+ reabsorption through PT NHE3	0.3	-
$\eta_{Na,\ reabs\text{-}PT,other}$	Fractional rate of PT Na+ reabsorption through non-NHE3, non-SGLT2 mechanisms	0.35	-
$\Phi_{Na,ALH0}$	Rate of sodium delivered to the ALH under baseline conditions	2.02*	µl/min
$\Phi_{Na,intake}$	Sodium intake rate	100	mEq/day
$\tau_{x,SGLT}$	Time constant for SGLT expression adaptation		
B	LoH flow dependence coefficient	0.75	-
C_{glu}	Plasma glucose concentration	5	mmol/L
$C_{albumin}$	Plasma albumin concentration	35	mg/dl
C_{prot}	Plasma protein concentration	7	g/dl
d_{aa0}	Nominal afferent arteriole diameter	11	µm
d_{ea0}	Nominal efferent arterial diameter	16.5	µm
$D_{c,cnt\text{-}cd}$	Connecting tubule/collecting duct effective diameter at control pressure	22	µm
$D_{c,dct}$	Distal convoluted tubule diameter at control pressure	17	µm
$D_{c,lh}$	Loop of Henle diameter at control pressure	17	µm
$D_{c,pt}$	Proximal tubule diameter at control pressure	27	µm
$J_{glu,s12}$	Rate of glucose reabsorption through SGLT2 in the PT S1 and S2 segment per unit length	0.2	mmol/min/ mm

$J_{glu,s3}$	Rate of glucose reabsorption through SGLT1 in the PT S3 segment per unit length	0.025	mmol/min/ mm
$K_{albumin0}$	Albumin sieving coefficient	0.06	%
K_{f0}	Glomerular ultrafiltration coefficient	4	L/min-mmHg
L_{aa}	Average afferent arteriole length	73.6*	µm
L_{ea}	Average efferent arteriole length	73.6*	µm
L_{CNT-CD}	Connecting tubule/collecting duct effective length	10	mm
L_{dct}	Distal convoluted tubule length	5	mm
$L_{LoH,Asc}$	Ascending loop of Henle length	10	mm
$L_{LoH,Desc}$	Descending loop of Henle length	10	mm
$L_{pt,s1}$	Length of the PT S1 segment	5	mm
$L_{pt,s2}$	Length of the PT S2 segment	5	mm
$L_{pt,s3}$	Length of the PT S3 segment	4	mm
$N_{nephrons}$	Number of nephrons	2e6	-
$[Na]_{ref}$	Normal blood/IF equilibrium sodium concentration	140	mmol/L
Na_{stored}	Maximum peripherally stored sodium	2000	Mmol
$P_{c,cnt-cd}$	CNT/CD control pressure	5	mmHg
$P_{c,dt}$	DCT control pressure	6	mmHg
$P_{c,lh,asc}$	Ascending loop of Henle control pressure	7	mmHg
$P_{c,lh,desc}$	Descending loop of Henle control pressure	8	mmHg
$P_{c,pt,s1}$	PT S1 segment control pressure	20.2	mmHg
$P_{c,pt,s2}$	PT S2 control pressure	15	mmHg
$P_{c,pt,s3}$	PT S3 control pressure	11	mmHg

Q_{water}	Rate constant for water transfer between blood and IF	1	1/min
Q_{Na}	Rate constant for sodium transfer between blood and IF	1	1/min
$Q_{Na,storage}$	Rate constant for sodium storage/release from the peripheral compartment	0.02	1/min
$R_{preaff,0}$	Nominal preafferent arteriole resistance	14	mmHg-min/L
$RC_{albumin}$	PT capacity for albumin reabsorption	1.7	pg/min/tubule
μ	Blood viscosity	5e-7	mmHg-min
$Water_{in}$	Water intake rate	2.1	L/day
$X_{sglt,max}$	Maximum increase in SGLT expression	30	%

*Value calculated based on other parameters under baseline conditions

Table S2. Regulatory mechanisms model parameters

Parameter	Definition	Value	Units
$\Phi_{Na,md,0}$	Setpoint for sodium flow delivered to the macula densa	0.885*	μl/min
$A_{md\text{-}renin}$	Scaling factor for macula densa renin secretion	0.9	-
$Aldo^{\cdot}$	Aldosterone concentration setpoint	85	pg/ml
AT1-bound-$AngII_0$	AT1-bound AngII setpoint	16.6*	pg/ml
$C_{NA,MD,0}$	Macula Densa sodium concentration setpoint	63.3*	mEq/L
$G_{CO\text{-}tpr}$	Proportional gain for cardiac output – TPR controller	0.1	-
$G_{Na\text{-}vp}$	Proportional gain for vasopressin control of sodium concentration	0.1	-
$K_{i\text{-}tpr}$	Integral gain for vasopressin control of sodium concentration	0.1	-

$K_{i\text{-}vp}$	Integral gain for vasopressin control of sodium concentration	0.005	-
$m_{aldo,cnt\text{-}cd}$	Slope factor for aldosterone effect on CNT/CD sodium reabsorption	0.5	-
$m_{aldo,dct}$	Slope factor for aldosterone effect on CNT/CD sodium reabsorption	0.5	-
$m_{AT1\text{-}aff}$	Slope factor for AT1-bound AngII effect on afferent resistance	16	-
$m_{AT1\text{-}eff}$	Slope factor for AT1-bound AngII effect on efferent resistance	16	-
$m_{AT1\text{-}preaff}$	Slope factor for AT1-bound AngII effect on preafferent resistance	16	-
$m_{AT1\text{-}pt}$	Slope factor for AT1-bound AngII effect on proximal tubule Na+ reabsorption	16	-
$m_{autoreg}$	Myogenic autoregulation slope factor	2	-
m_{TGF}	Tubuloglomerular feedback signal slope factor	6	-
$P_{preafferent,0}$	Preafferent arteriole pressure setpoint	71*	mmHg
$RIHP_0$	Renal interstitial hydrostatic pressure setpoint	9.66*	mmHg
$S_{aldo\text{-}cnt\text{-}cd}$	Scaling factor for aldosterone effect on CNT/CD sodium reabsorption	0.2	-
$S_{aldo\text{-}dct}$	Scaling factor for aldosterone effect on DCT sodium reabsorption	0.05	-
$S_{AT1\text{-}aldo}$	Scaling factor for AT1-bound AngII effect on aldosterone secretion	0.02	-
$S_{AT1\text{-}aff}$	Scaling factor for AT1-bound AngII effect on afferent resistance	0.8	-
$S_{AT1\text{-}eff}$	Scaling factor for AT1-bound AngII effect on efferent resistance	0.8	-

$S_{AT1\text{-}preaff}$	Scaling factor for AT1-bound AngII effect on preafferent resistance	0.8	-
$S_{AT1\text{-}pt}$	Scaling factor for AT1-bound AngII effect on proximal tubule Na+ reabsorption	0.1	-
$S_{autoreg}$	Preafferent autoregulation signal scaling factor	1	-
S_{TGF}	Tubuloglomerular feedback signal scaling factor	0.7	-
$S_{P\text{-}N,CNT\text{-}DC}$	CNT-DC pressure-natriuresis signal scaling factor	0.5	-
$S_{P\text{-}N,DCT}$	DCT pressure-natriuresis signal scaling factor	0.1	-
$S_{P\text{-}N,LoH}$	LoH pressure-natriuresis signal scaling factor	0.1	-
$S_{P\text{-}N,PT}$	PT pressure-natriuresis signal scaling factor	0.5	-

Table S3. Renin Angiotensin Aldosterone System model parameters

Parameter	Definition	Value	Units
ACE	ACE activity	47.65*	/min
Chymase	Chymase activity	2.5*	/min
K_{AT1}	AT1-receptor binding rate	12.1*	/min
K_{AT2}	AT2-receptor binding rate	4*	/min
$K_{d,AngI}$	AngI degradation rate	0.0924	/min
$K_{d,AngI}$	AngII degradation rate	0.146	/min
$K_{d,AT1}$	AT1-bound AngII degradation rate	3.47	/min
$K_{d,renin}$	Renin degradation rate	4	/min

Table S4. Renal Disease Model Parameters

Parameter	Definition	Value	Units	Eq.
ΔSA_{max}	Maximal glomerular surface area increase	50	%	30
$\Delta Perm$	Decrease in glomerular membrane permeability	0	%	31
γ	Hill coefficient for glomerular pressure effect on podocyte injury	2	-	32
$\mu_{other,seiv}$	Podocyte damage due to non-hemodynamic factors	0	-	33
τ_{SA}	Time constant for glomerular hypertrophy			30
E_{max}	Maximum fold increase in sieving coefficient due to glomerular pressure	4	-	32
$K_{m,gp,seiv}$	Glomerular pressure difference that elicits half the maximal effect on albumin seiving	25	mmHg	32
P_{GC0}	Glomerular hydrostatic pressure above which podocyte injury occurs	65	mmHg	29
$X_{sglt,max}$	Maximum increase in SGLT expression	30	%	26

Table S5. Model Initial Conditions

Variable	Definition	Value	Units
AngI	Angiotensin I	8.164*	pg/mg
AngII	Angiotensin II	5.17*	pg/mg
AT1-bound AngII	AT1-bound AngII	16.6*	pg/mg
AT2-bound AngII	AT2-bound AngII	5.5*	pg/mg
CO	Cardiac Output	5	L/min
BV	Blood Volume	5	L
IFV	Interstitial Fluid Volume	12	L
Na_{blood}	Blood sodium amount	700	mEq
Na_{IF}	Interstitial sodium amount	1400	mEq
Na_{stored}	Stored sodium amount	0	mEq
PRC	Plasma Renin Concentration	17.84	pg/ml